The Cryosphere, 11, 1015–1033, 2017
www.the-cryosphere.net/11/1015/2017/
doi:10.5194/tc-11-1015-2017

The Cryosphere Open Access EGU

Reconstructions of the 1900–2015 Greenland ice sheet surface mass balance using the regional climate MAR model

Xavier Fettweis[1], Jason E. Box[2], Cécile Agosta[1], Charles Amory[1], Christoph Kittel[1], Charlotte Lang[1], Dirk van As[2], Horst Machguth[3,4], and Hubert Gallée[5]

[1]Laboratory of Climatology, Department of Geography, University of Liège, Liège, Belgium
[2]Department of Glaciology and Climate, Geological Survey of Denmark and Greenland (GEUS), Copenhagen, Denmark
[3]Department of Geography, University of Zurich, Zurich, Switzerland
[4]Department of Geosciences, University of Fribourg, Fribourg, Switzerland
[5]Laboratoire de Glaciologie et Géophysique de l'Environnement (LGGE), Grenoble, France

Correspondence to: Xavier Fettweis (xavier.fettweis@ulg.ac.be)

Received: 17 November 2016 – Discussion started: 21 November 2016
Revised: 22 March 2017 – Accepted: 23 March 2017 – Published: 25 April 2017

Abstract. With the aim of studying the recent Greenland ice sheet (GrIS) surface mass balance (SMB) decrease relative to the last century, we have forced the regional climate MAR (Modèle Atmosphérique Régional; version 3.5.2) model with the ERA-Interim (ECMWF Interim Re-Analysis; 1979–2015), ERA-40 (1958–2001), NCEP–NCARv1 (National Centers for Environmental Prediction–National Center for Atmospheric Research Reanalysis version 1; 1948–2015), NCEP–NCARv2 (1979–2015), JRA-55 (Japanese 55-year Reanalysis; 1958–2014), 20CRv2(c) (Twentieth Century Reanalysis version 2; 1900–2014) and ERA-20C (1900–2010) reanalyses. While all these forcing products are reanalyses that are assumed to represent the same climate, they produce significant differences in the MAR-simulated SMB over their common period. A temperature adjustment of $+1\,^{\circ}\mathrm{C}$ (respectively $-1\,^{\circ}\mathrm{C}$) was, for example, needed at the MAR boundaries with ERA-20C (20CRv2) reanalysis, given that ERA-20C (20CRv2) is $\sim 1\,^{\circ}\mathrm{C}$ colder (warmer) than ERA-Interim over Greenland during the period 1980–2010. Comparisons with daily PROMICE (Programme for Monitoring of the Greenland Ice Sheet) near-surface observations support these adjustments. Comparisons with SMB measurements, ice cores and satellite-derived melt extent reveal the most accurate forcing datasets for the simulation of the GrIS SMB to be ERA-Interim and NCEP–NCARv1. However, some biases remain in MAR, suggesting that some improvements are still needed in its cloudiness and radiative schemes as well as in the representation of the bare ice albedo.

Results from all MAR simulations indicate that (i) the period 1961–1990, commonly chosen as a stable reference period for Greenland SMB and ice dynamics, is actually a period of anomalously positive SMB ($\sim +40\,\mathrm{Gt\,yr^{-1}}$) compared to 1900–2010; (ii) SMB has decreased significantly after this reference period due to increasing and unprecedented melt reaching the highest rates in the 120-year common period; (iii) before 1960, both ERA-20C and 20CRv2-forced MAR simulations suggest a significant precipitation increase over 1900–1950, but this increase could be the result of an artefact in the reanalyses that are not well-enough constrained by observations during this period and (iv) since the 1980s, snowfall is quite stable after having reached a maximum in the 1970s. These MAR-based SMB and accumulation reconstructions are, however, quite similar to those from Box (2013) after 1930 and confirm that SMB was quite stable from the 1940s to the 1990s. Finally, only the ERA-20C-forced simulation suggests that SMB during the 1920–1930 warm period over Greenland was comparable to the SMB of the 2000s, due to both higher melt and lower precipitation than normal.

1 Introduction

Since the end of the 1990s, the Greenland ice sheet (GrIS) has been losing mass as a result of both surface meltwater run-off increase (representing $\sim 60\,\%$ of the mass loss)

and iceberg discharge increase (van den Broeke et al., 2016). This recent acceleration of the ice dynamics is likely a consequence of the increase of meltwater availability and ocean warming, although the role of meltwater remains unclear (Sundal et al., 2011; Tedstone et al., 2013; de Fleurian et al., 2016). The recent surface melt increase likely results from global warming, enhanced by the Arctic amplification (Serreze and Barry, 2011) and general circulation-observed changes in summer favouring advection of warm air masses over GrIS (Fettweis et al., 2013a; Hanna et al., 2016). In view of the impact of GrIS on the observed global sea level rise (van den Broeke et al., 2016), it is important to consider this recent surface mass loss in a longer perspective.

The warming observed in the 1930s (Chylek et al., 2006) is, for example, often mentioned as equivalent to the warming observed since the end of the 1990s, suggesting that the recent surface mass loss may not be unprecedented in the 100-yr Greenland climate history. A first estimation of the surface mass balance (SMB) through the entire previous century has been made by Fettweis et al. (2008), Hanna et al. (2011) and more recently by Box (2013), based mainly on observations and statistical regressions and corrections. However, the number of in situ observations is too sparse over Greenland before 1950 to build reconstructions at the daily time scale as in Mernild and Liston (2013), and many uncertainties remain in the available reconstructions, whose time scales are monthly at best. The recent development of a new reanalysis dataset covering the entire last century and constrained by observations from both Greenland and outside Greenland offers a new opportunity to evaluate SMB over GrIS through the last century (Hanna et al., 2011). Regional climate models (RCMs) especially developed for polar regions (Rae et al., 2012) and coupled with complex snow models are powerful tools to physically downscale the 6-hourly reanalyses and estimate SMB. Both the spatial resolution and the snow model used in reanalyses are not yet adequate to directly derive SMB from reanalyses (Cullather et al., 2016). Among the "polar" RCMs, there is the MAR (Modèle Atmosphérique Régional) model, fully coupled with a snow energy balance model and developed and extensively evaluated to study the present Greenland climate as well as to perform future projections of GrIS SMB for the last IPCC report (Fettweis et al., 2013b).

In the present paper, we force the MAR model with eight reanalyses over Greenland at a resolution of 20 km for the period 1900–2015 to (i) evaluate the uncertainties coming from reanalyses in RCM-based reconstructions (while reanalyses are assumed to represent exactly the same climate) and (ii) estimate SMB before 1950 with two new reanalyses covering the entire century. All previous RCM-based SMB estimations use the ECMWF (European Centre for Medium-Range Weather Forecasts) reanalysis as forcing until now and cover only the second half of the last century (e.g. Lucas-Picher et al., 2012; Rae et al., 2012; Noël et al., 2016).

After a brief description of the MAR model and reanalyses used as forcing in Sect. 2, Sect. 3 compares the eight reanalyses used for MAR forcing over Greenland as well as the reanalysis-forced MAR results over our reference period (1980–1999). In Sect. 4, we present a validation over 1958–2010 of the eight MAR-based series vs. in situ observations from ablation stakes, ice cores and satellite-derived melt extent. Finally, Sect. 5 discusses the time evolution of the GrIS SMB since 1900 as well as the uncertainties coming from the reanalyses.

2 Data

2.1 The MAR model

The version of MAR used here is 3.5.2 (called MAR hereafter) and has been used by Colgan et al. (2015), Alexander et al. (2016), Koenig et al. (2016), Schlegel et al. (2016) and Wyard et al. (2017). See Fettweis (2007), Reijmer et al. (2012) and Fettweis et al. (2013b) for a detailed description of the MAR model and its surface scheme SISVAT (soil ice snow vegetation atmosphere transfer) dealing with the energy and mass exchanges between surface, snow and atmosphere. Compared to version 2 of MAR (hereafter MARv2) and the set-ups used in Fettweis et al. (2013b), the following changes were implemented.

- A resolution of 20 km (instead of 25 km) as well as the GrIS topography from Bamber et al. (2013) (instead of Bamber et al., 2001) were used here. In addition, to each atmospheric MAR $20 \times 20\,km^2$ grid cell, we associated two sub-grid cells covered by tundra and permanent ice according to the Bamber et al. (2013) ice mask. This fractional ice sheet mask in MARv3.x allows the computation of SMB outside the original MAR ice sheet mask (with the aim of forcing ice sheet models at higher resolutions), and a grid cell will be considered hereafter as an ice sheet grid cell if its permanent ice cover is higher than 50 %. In addition, when integrated over the whole ice sheet, the surface mass values will be weighted by the permanent ice cover of each grid cell (i.e. for cells at least 50 % covered by permanent ice).

- According to the MAR bare ice albedo overestimation found by Alexander et al. (2014) using MARv3.2, the bare ice albedo has been improved in MARv3.5.2 by exponentially varying between 0.4 (dirty ice) and 0.55 (clean ice) as a function of the accumulated surface water height and slope. For densities lower than $550\,kg\,m^{-3}$, the CROCUS snow model albedo (Brun et al., 1992) is used with a minimum albedo value set to 0.7. Concerning snowpack with surface density higher than $550\,kg\,m^{-3}$ (representing the maximum density of pure snow), the minimum allowed albedo is a linear

function with a smooth transition between the minimum pure snow albedo (0.7) and clean ice albedo (0.55).

– Vernon et al. (2013) emphasized an overestimation of accumulation simulated by MARv2 in the interior of the ice sheet. This bias was in part corrected in MARv3.5.2 by slightly increasing the snowfall velocity, which enabled more precipitation along the ice sheet margin and less inland.

– Finally, MARv3.5.2 is now parallelized with OpenMP, its outputs are CORDEX compliant and some usual bug corrections have been made since MARv2.

2.2 Reanalyses

In this study, we use the reanalyses listed below to force MAR every 6 h at its lateral atmospheric boundaries (temperature, humidity, wind and pressure at each vertical MAR level) and over oceanic grid cells (sea ice cover, SIC, and sea surface temperature, SST).

– ERA-Interim (ECMWF Interim Re-Analysis) over 1979–2015, available at a resolution of $\sim 0.75°$ from ECMWF. As in Fettweis et al. (2013b), this state-of-the-art third generation reanalysis is used as reference over our chosen reference period (1980–1999) and assimilates the greatest fraction of the in situ and remote observations available (Dee et al., 2011).

– ERA-40 over 1958–2001 (resolution: $\sim 1.125°$), the second generation reanalysis from ECMWF (Uppala et al., 2005). One of main differences between ERA-40 and ERA-Interim is a fully revised humidity scheme in ERA-Interim (Dee et al., 2011), which impacts the snowfall amount simulated by MAR as shown by Fettweis et al. (2013b).

– ERA-20C over 1900–2010 (resolution: $\sim 1.25°$), the latest generation of ECMWF reanalysis products assimilating only surface pressures and near-surface winds over the ocean surface but starting in 1900 (Poli et al., 2016). As this reanalysis assimilates much less data than ERA-40 and ERA-Interim, it is generally less reliable than the other ECMWF reanalyses, but its reliability increases with time with the increasing amount of assimilated observations.

– NCEP–NCARv1 (National Centers for Environmental Prediction–National Center for Atmospheric Research reanalysis version 1; referred to as NCEPv1 here) over 1948–2015 (resolution: 2.5°), First generation reanalysis from the NCEP–NCAR covering the second half of the last century at low spatial resolution (Kalnay et al., 1996).

– NCEP–DOE (NCEP–Department of Energy; referred to as NCEPv2 here) over 1979–2015 (resolution: 2.5°), second generation reanalysis using an improved version of the NCEP–NCARv1 global model and assimilating additional satellite data with respect to NCEP–NCARv1 (Kanamitsu et al., 2002).

– 20CRv2 over 1871–2012 (resolution: 2.0°), experimental reanalysis based on an ensemble mean of 56 members assimilating only surface pressure, monthly sea surface temperature and sea ice cover (Compo et al., 2011). Only outputs after 1900 were used here. As for ERA-20C, its reliability increases with time (i.e. with the amount of assimilated data).

– 20CRv2c over 1851–2014 (resolution: 2.0°), same as 20CRv2 but correcting a bias found in the sea ice distribution by assimilating new SST and SIC data.

– JRA-55 (Japanese 55-year Reanalysis) over 1958–2014 (resolution: 1.25°), second generation reanalysis from the Japan Meteorological Agency, described in Kobayashi et al. (2015).

3 Evaluation over 1980–1999

3.1 MAR forcings

In Fettweis et al. (2013b), summer temperatures at 600 hPa, geopotential height at 500 hPa and wind speed at 500 hPa from the different MAR forcing fields were compared over 1980–1999 to explain the discrepancies between the MAR simulations using different forcings.

According to Fettweis et al. (2013a), the JJA (June–July–August) mean 700 hPa (T700) or 600 hPa temperatures (T600) in the free atmosphere over Greenland are a good predictor of the melt variability in MAR. Therefore, temperature biases at the MAR boundaries will directly impact the amount of melt simulated by MAR (Fettweis et al., 2013b). Since free atmosphere temperatures are not assimilated either in 20CRv2c or in ERA-20C reanalysis, a comparison of this field is presented in Fig. 1 over our reference period (1980–1999), which is covered by all datasets used here and during which SMB has been relatively stable. While SMB has already started to decrease at the end of the 1990s, a comparison over a period longer than 20 years does not change the conclusions of this comparison as justified in Fettweis et al. (2013b).

The mean 1980–1999 free atmosphere JJA temperature from ERA-40 and NCEPv1 compares very well with ERA-Interim over Greenland (see Fig. 1b and e). Surprisingly, the second generation of the NCEP reanalysis does not compare as well as with ERA-Interim and NCEPv1 because NCEP2 is too warm in summer, except in the vicinity of Iceland (see Fig. 1f). As specific humidity (used as forcing at the MAR lateral boundaries) needs to be derived from relative humid-

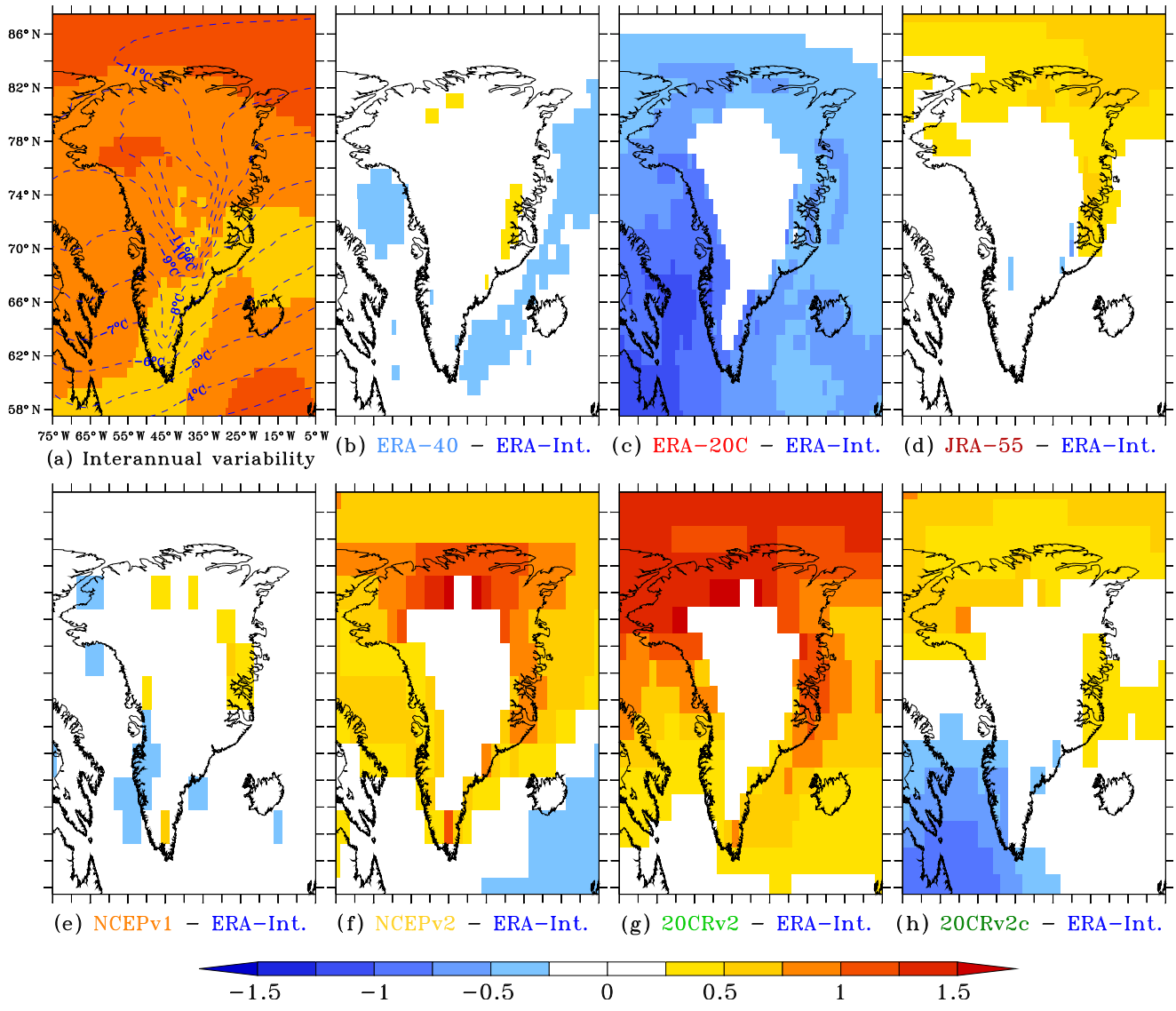

Figure 1. (a) In the background, the interannual variability (i.e. standard deviation) of the JJA mean 700 hPa temperature (T700) is simulated by ERA-Interim over 1980–1999. Units are °C. The contours of the mean JJA T700 are plotted in dashed blue. **(b)–(h)** Mean anomalies of the JJA 700 hPa temperature simulated by the different reanalyses used in this study with respect to ERA-Interim over 1980–1999 (in °C). No comparison is shown above 2000 m a.s.l. due to the aim of only showing comparisons in the free atmosphere (700 hPa), and the datasets are shown here by using their native lat–long projection. Similar figures over different reference periods and at other vertical levels (850 and 500 hPa) can be found in the Supplement.

ity in NCEPv2, these temperature biases impact the precipitation amount simulated by MAR forced by NCEPv2.

The reanalyses covering the entire 20th century are significantly ($> 1\,^{\circ}C$) warmer (20CRv2, Fig. 1g) and colder (ERA-20c, Fig. 1c) than ERA-Interim in summer. Similar anomalies also occur in winter and at other vertical levels (see Figs. S1–S4 of the Supplement). In view of these biases in 20CRv2 and ERA-20C, a correction of $-1\,^{\circ}C$ ($+1\,^{\circ}C$) was applied to the temperature fields from these two reanalyses at each vertical level of the MAR lateral boundaries while keeping the relative humidity constant. These corrected reanalyses are called CORR-20CRv2 and CORR-ERA-20c hereafter. These corrections aim at having a good agreement with the ERA-Interim-forced MAR melt rate over the last decades for a better comparison between the recent melt increase and past conditions. Indeed, as the melt response to a temperature anomaly is not linear (Fettweis et al., 2013b), inaccurate current melt rates bias melt anomalies in the past. It should be noted that no change was applied to the MAR oceanic boundaries (SST and SIC) and that the temperatures corrections were homogeneously applied through the whole year and over the entire period covered by these two reanalyses,

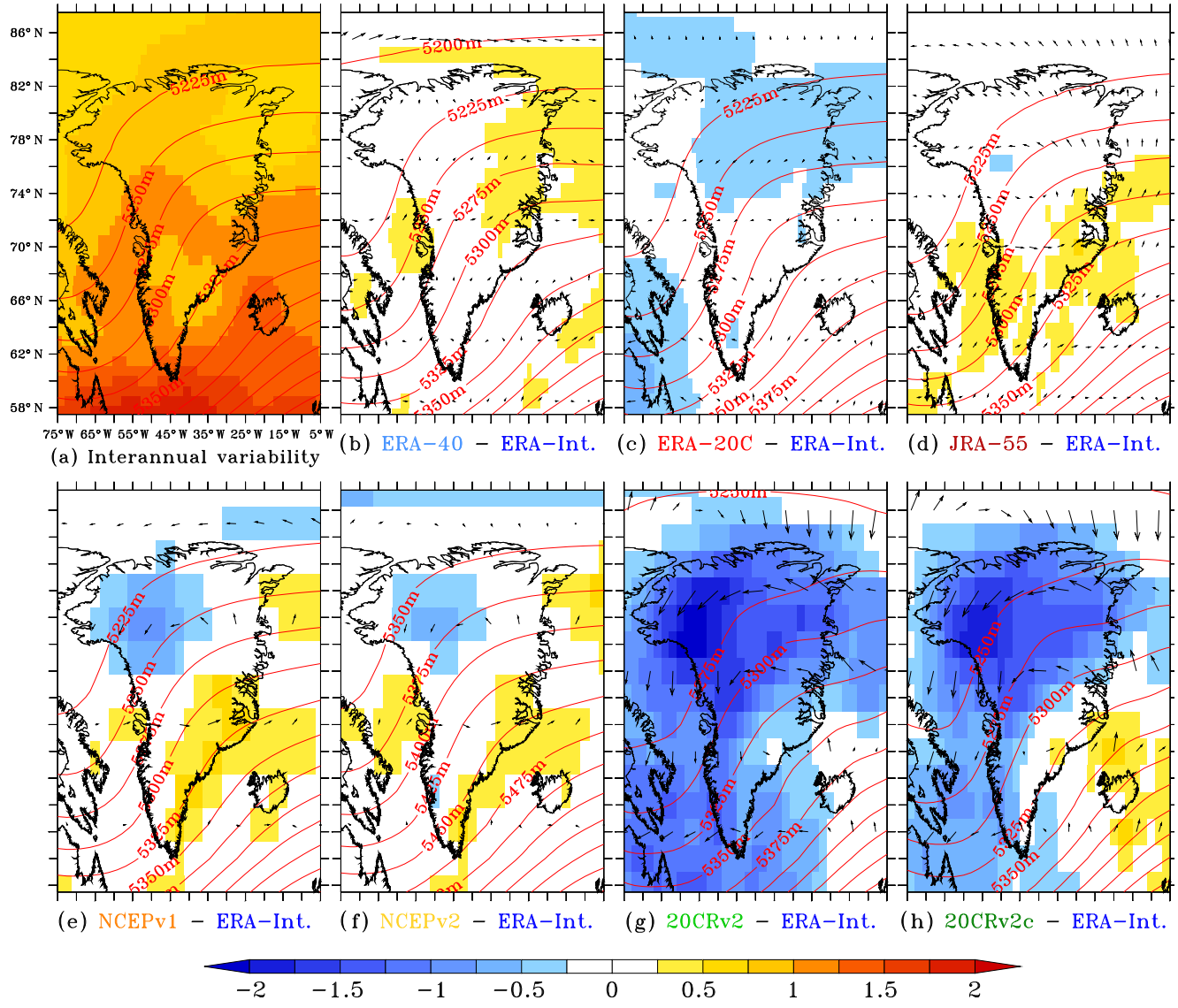

Figure 2. Idem as Fig. 2, but for the mean annual geopotential height (Z500) at 500 hPa over 1980–1999. Units are metres. The wind vectors represent anomalies of wind field.

as these biases are constant in time over 1948–2010 with respect to NCEPv1 (see Figs. S1–S4 of the Supplement). As we will see in Sect. 4.1, these temperature corrections enable a better comparison of MAR with in situ temperature measurements than with unmodified 20CRv2 and ERA-20C-based fields as lateral boundaries. Finally, as the warm bias from 20CRv2 is partly corrected in 20CRv2c and is now centred around zero on average with a too-warm atmosphere at the north of Greenland and too cold at the south-west, unmodified 20CRv2c temperatures are then used to force MAR at its lateral boundaries.

Since the surface pressure has been assimilated in all reanalyses used here, the general circulation (gauged here by the 500 hPa geopotential height in Fig. 2) including the North Atlantic Oscillation (NAO) compares well over the recent decades (Belleflamme et al., 2013), except for 20CRv2(c), which underestimates wind speed at 500 hPa, inducing anticlockwise circulation anomalies over Greenland (see Fig. 2g and h). Moreover, as a consequence of the lack of (or less reliable) assimilated data before 1940, the general circulation variability from 20CRv2 and ERA-20C diverges according to Belleflamme et al. (2013) and explains the discrepancies between MAR forced by 20CRv2(c) and ERA-20C before 1940 (see Sect. 6).

3.2 MAR results

Considering their interannual variability, the mean SMB components from the different MAR simulations compare

Table 1. Average and standard deviation (gauging the interannual variability) of the annual SMB components simulated by MAR over 1980–1999 and from Box's reconstruction (Box, 2013; interpolated to the MAR 20 km grid). Units are GT yr^{-1} and the acronym of each simulation ($RCM_{forcings}$) is given in the first column. The surface mass balance (SMB) equation is SMB = snowfall + rainfall − run-off − water fluxes. The run-off is the fraction of water from both surface melt and rainfall that is not refrozen before reaching the ocean.

Simulation acronym	SMB	Snowfall	Rainfall	Run-off	Water fluxes	Meltwater
$MAR_{ERA-Interim}$	480 ± 87	683 ± 56	28 ± 5	220 ± 52	12 ± 4	427 ± 82
MAR_{ERA-40}	529 ± 89	716 ± 57	31 ± 6	210 ± 54	9 ± 3	418 ± 86
$MAR_{ERA-20C}$	500 ± 71	624 ± 76	18 ± 4	126 ± 35	15 ± 3	296 ± 59
$MAR_{CORR-ERA-20c}$	491 ± 84	665 ± 59	26 ± 6	190 ± 48	10 ± 3	399 ± 77
MAR_{NCEPv1}	467 ± 88	675 ± 59	28 ± 6	228 ± 53	8 ± 4	440 ± 82
MAR_{NCEPv2}	486 ± 86	672 ± 60	22 ± 5	200 ± 46	8 ± 4	409 ± 74
MAR_{20CRv2}	420 ± 102	703 ± 60	31 ± 6	221 ± 52	12 ± 2	432 ± 82
$MAR_{CORR-20CRv2}$	459 ± 88	670 ± 57	22 ± 4	309 ± 67	5 ± 5	559 ± 102
$MAR_{20CRv2c}$	456 ± 92	680 ± 59	25 ± 6	241 ± 63	8 ± 4	462 ± 97
MAR_{JRA-55}	482 ± 88	670 ± 57	29 ± 5	209 ± 52	9 ± 4	412 ± 83
Box (2013)	502 ± 74	735 ± 62		229 ± 47		424 ± 71

very well with each other when they are integrated over the entire ice sheet, except for the non-corrected ERA-20C and 20CRv2-forced MAR simulations (see Table 1). However, when looking at spatial differences (see Figs. 3 and 4), the comparison with the $MAR_{ERA-Interim}$ simulation over 1980–1999 shows the following.

1. MAR_{ERA-40} slightly overestimates precipitation because the ERA-40 high atmosphere is wetter than ERA-Interim, as a result of biases in the ERA-40 humidity scheme that were later corrected in ERA-Interim (Dee et al., 2011). However, this wet anomaly is homogeneous over the whole integration domain and explains why there are no locally significant discrepancies between $MAR_{ERA-Interim}$ and MAR_{ERA-40}.

2. Although the temperature corrections of $+1°$ degree at the MAR lateral boundaries reduce the underestimation of melt by $MAR_{ERA-20c}$, $MAR_{CORR-ERA-20c}$ is still too cold in summer. Both ERA-20C-forced simulations also significantly underestimate precipitation along the south-western coast (60–70° N) because not enough humidity is advected at the south-west lateral boundaries of our integration domain, from where the prevailing flow over south Greenland comes. This too-dry and cold main flux is a consequence of the ERA-20 underestimation of the free atmosphere temperature and wind speed in this area (see Figs. 1c and 2c).

3. Most of the differences between $MAR_{ERA-Interim}$ and MAR_{NCEPv1} (MAR_{JRA-55}) are within the interannual variability of $MAR_{ERA-Interim}$ over 1980–1999 and are therefore insignificant. We can see an underestimation of precipitation along the south-east coast with respect to $MAR_{ERA-Interim}$, but it is not significant.

4. MAR_{NCEPv2} is too wet (too dry) in the south-west (south-east) of the ice sheet despite the fact that the general circulation (here Z500) from NCEPv2 compares very well with ERA-Interim. However, NCEPv2 is too warm (too cold) in the south-west (south-east) of Greenland, which impacts the amount of humidity advected by MAR from its lateral boundaries. This is because the specific humidity is derived from the NCEPv2 relative humidity and is then affected by the temperature biases found in NCEPv2 with respect to ERA-Interim.

5. The patterns of anomalies of $MAR_{CORR-20CRv2}$ and $MAR_{20CRv2c}$ with respect to $MAR_{ERA-Interim}$ are similar and mainly result from anomalies in precipitation. We can see that the temperature correction in CORR-20CRv2 reduces the MAR_{20CRv2} run-off overestimation vs. $MAR_{CORR-20CRv2}$, but this correction does not impact the simulated MAR precipitation: $MAR_{20CRv2(c)}$ is too wet (dry) along the north-eastern (north-western) coast, as a result of the anti-clockwise circulation anomalies simulated by 20CRv2(c) with respect to ERA-Interim (see Fig. 2). Finally, except along the south-western margin where CORR-20CRv2 and 20CRv2c are too cold in summer, $MAR_{CORR-20CRv2}$ and $MAR_{20CRv2c}$ weakly overestimate run-off with respect to $MAR_{ERA-Interim}$.

4 Validation

4.1 Near-surface climate

As validation of the near-surface conditions simulated by MAR, a comparison with daily measurements from the automatic weather station (AWS) of the PROMICE (Programme for Monitoring of the Greenland Ice Sheet) net-

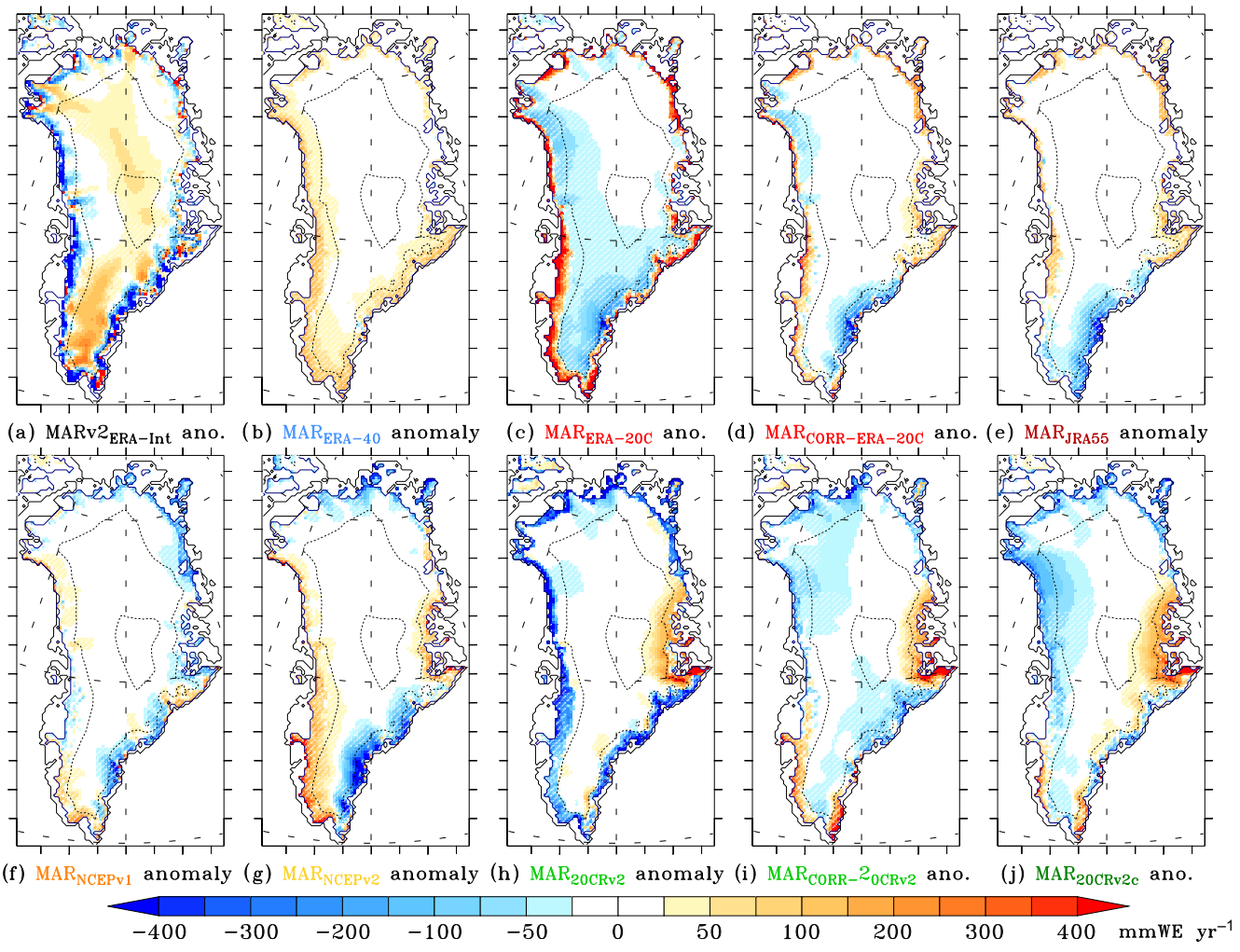

Figure 3. **(a)** Difference between the mean annual SMB (in mm.w.e. yr^{-1}) simulated by MARv2 forced by ERA-Interim and MARv3.5.2 forced by ERA-Interim over 1980–1999. **(b)** Difference between the mean 1980–1999 annual SMB simulated by MARv3.5.2 forced by ERA-40 and simulated by MARv3.5.2 forced by ERA-Interim. **(c)** Idem as **(b)** but for ERA-20C. **(c)** Idem as **(b)** but for CORR-ERA-20c. **(e)** Idem as **(b)** but for JRA-55. **(f)** Idem as **(b)** but for NCEPv1. **(g)** Idem as **(b)** but for NCEPv2. **(h)** Idem as **(b)** but for 20CRv2. **(i)** Idem as **(b)** but for CORR-20CRv2. **(j)** Idem as **(b)** but for 20CRv2c. Finally, the areas where the differences are lower than the interannual variability of MARv3.5.2 forced by ERA-Interim over 1980–1999 are hatched.

work (Ahlstrom et al., 2008) starting in mid-2007 is presented over the common period covered by the forcing datasets used here: 2008–2010. The raw PROMICE data are used here without any filtering or withdrawing of aberrant values. The MAR values at each station are based on an interpolation of the four nearest MAR grid cells weighted by the inverse distance to the station. As the elevation difference between MAR and AWS is not corrected, the comparison is only carried out on the 12 AWSs listed in Table S1 of the Supplement that have an elevation difference within 100 m of the interpolated MAR 20 km topography. Scatter plots are shown in Fig. 5 and statistics are listed in Table 2.

On average for the 12 AWSs, the comparison of $MAR_{ERA-Interim}$ with the measured daily near-surface temperature is excellent, with a correlation above 0.96 and a RMSE (root mean square error) of 2–3 °C, representing less than 30 % of the daily variability. The improvements with respect to MARv2 are evident. The biases with the downward shortwave (longwave) radiation remain, however, high in both MAR versions, with the RMSE representing 25 % (70 %) of the daily variability of these fluxes. Due to an underestimation of the cloudiness, MAR slightly overestimates (highly underestimates) downward shortwave (longwave) radiation. Such biases in the short- and longwave were also found in the regional RACMO2.3 model (Van Tricht et al., 2016), suggesting that improvements are still needed in the clouds and/or radiative schemes of (regional) climate models. As a result, $MAR_{ERA-Interim}$ is

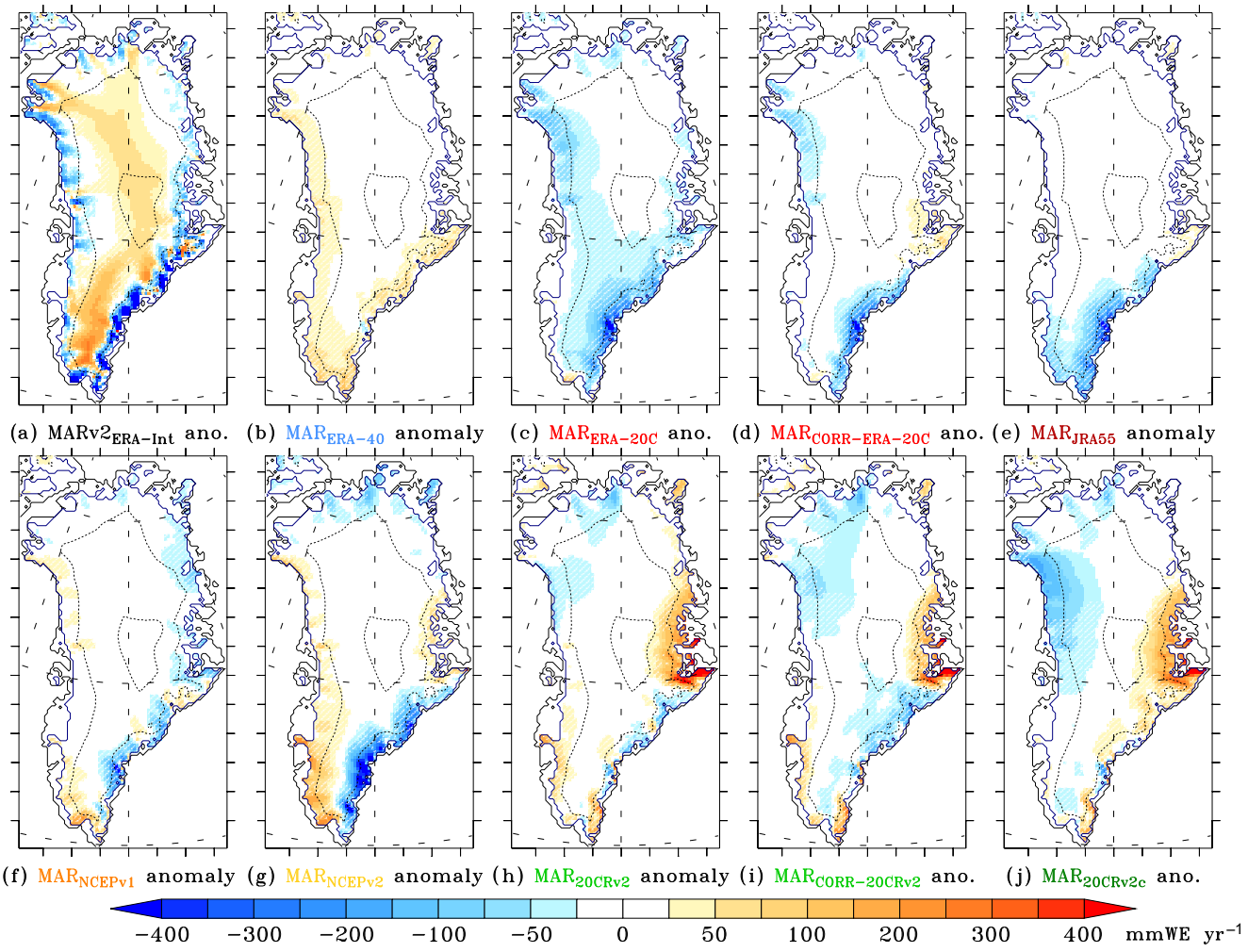

Figure 4. Same as Fig. 3 but for snowfall (in mm.w.e. yr^{-1}).

slightly too cold (−0.29 °C at the annual scale), in particular in summer (−0.65 °C) when the underestimation of the downward infrared flux is the highest (a bias of −18 W m^{-2} compared with a daily variability of 43 W m^{-2}). Finally, MAR overestimates the bare ice albedo as it is limited to 0.40 in MARv3.5.2, while values ranging from 0.2 to 0.4 (due to the presence of impurities not taken into account into MAR) are observed in some PROMICE AWSs (Tedesco et al., 2016). In view of the sensitivity of the simulated SMB to the bare ice albedo formulation (van Angelen et al., 2012; Tedesco et al., 2016), improving its representation in MAR should be a priority for future developments.

Using other reanalyses than ERA-Interim as boundaries forcing does not significantly change the comparison of MAR with the PROMICE measurements. Table 2 shows the relevance of the ERA-20C temperature correction while the warm bias of 20CRv2 mitigates the cold bias found in $MAR_{ERA-Interim}$. Statistically, $MAR_{ERA-Interim}$ and MAR_{JRA-55} show the best agreement with PROMICE, whereas MAR_{20CRv2} shows the worst.

4.2 Surface mass balance

As validation of the SMB simulated by MAR over 1958–2010 (the period covered by seven of the datasets here), we use the following.

1. The ice core measurements in the accumulation area from Bales et al. (2001, 2009) and Ohmura et al. (1999). The MAR accumulations values (here in m.w.e. yr^{-1}) for each of the 246 records are averaged over the years listed in the three previous references (the mean from 1958–2010 is used if the period is not given or before 1958) and come from an interpolation of the four nearest inverse-distance-weighted MAR grid cells.

2. The new SMB database (hereafter MACHGUTH16) compiled under the auspice of PROMICE and available through the PROMICE web portal (http://www.

Table 2. Mean correlation, bias, RMSE and correlation over the 12 AWSs listed in Table S1 of the Supplement between MAR forced by the different reanalyses and daily observations from the PROMICE network over 2008–2010. Statistics are given for the surface pressure (SP), near-surface temperature (TAS) over the entire year and for the summer months only (for JJA; Summer TAS), shortwave downward flux (SWD) and longwave downward flux (SWD).

Simulation acronym	SP	TAS (°C)			Summer TAS (°C)		
	CORR	BIAS	RMSE	CORR	BIAS	RMSE	CORR
$MAR_{ERA-Interim}$	0.99	−0.29	2.32	0.96	−0.65	2.38	0.95
$MAR_{ERA-20C}$	0.99	−1.04	2.78	0.95	−1.42	2.92	0.93
$MAR_{CORR-ERA-20c}$	0.99	−0.26	2.56	0.95	−0.61	2.64	0.93
MAR_{NCEPv1}	0.99	−0.04	2.48	0.95	−0.26	2.47	0.93
MAR_{NCEPv2}	0.99	−0.19	2.52	0.95	−0.44	2.51	0.93
MAR_{20CRv2}	0.98	0.30	3.16	0.92	−0.27	3.07	0.90
$MAR_{CORR-20CRv2}$	0.98	−0.42	3.21	0.92	−1.02	3.25	0.89
$MAR_{20CRv2c}$	0.98	−0.33	3.09	0.93	−0.76	3.05	0.91
MAR_{JRA-55}	0.99	−0.56	2.51	0.96	−1.08	2.62	0.94
$MARv2_{ERA-Interim}$	0.99	−0.98	2.73	0.95	−1.39	2.90	0.94
Simulation acronym		SWD ($W\,m^{-2}$)			LWD ($W\,m^{-2}$)		
		BIAS	RMSE	CORR	BIAS	RMSE	CORR
$MAR_{ERA-Interim}$		3.42	27.07	0.96	−16.92	28.13	0.84
$MAR_{ERA-20C}$		4.05	30.54	0.96	−19.98	32.35	0.79
$MAR_{CORR-ERA-20c}$		3.17	30.43	0.96	−16.33	30.29	0.79
MAR_{NCEPv1}		1.84	29.58	0.96	−14.19	29.64	0.79
MAR_{NCEPv2}		2.70	29.74	0.96	−14.64	30.10	0.79
MAR_{20CRv2}		1.75	33.51	0.95	−14.28	32.55	0.74
$MAR_{CORR-20CRv2}$		0.21	32.30	0.95	−14.34	32.54	0.74
$MAR_{20CRv2c}$		0.73	32.21	0.95	−14.28	32.55	0.74
MAR_{JRA-55}		3.71	26.92	0.96	−17.98	29.41	0.83
$MARv2_{ERA-Interim}$		−1.8	27.64	0.95	−19.52	31.42	0.81

promice.dk) containing a total of ∼ 3000 measurements from 46 sites from 1892 to 2015 and mostly covering the ablation area of the GrIS and local glaciers (Machguth et al., 2016). For each site, the MAR SMB value is corrected as a function of the elevation difference between the MACHGUTH16 database and the interpolated MAR 20 km topography using a local and time varying SMB vs. elevation gradient as explained in Franco et al. (2012). Moreover, the MAR values (here in m.w.e.) are an integration of daily MAR outputs over the exact period given for each record in the MACHGUTH16 database. The data are not converted to m.w.e. yr^{-1}, as some MACHGUTH16 records sometimes cover only several months in the melt season. Only the records included in the 1958–2010 period with an elevation difference with the MAR topography of less than 500 m and inside the MAR ice sheet mask are considered here. The comparison is therefore limited to 1616 records from the MACHGUTH16 database (Machguth et al., 2016). Similarly, the same dataset has also been used in Noël et al. (2016) for the validation of RACMO2.3.

3. The revised version (fully described in Kjeldsen et al., 2015) of the 5 km reconstruction of the near-surface air temperature and the land ice SMB from Box (2013), hereafter BOX13, spanning 1840–2012 and calibrated to outputs from RACMO2.1/GR forced by ERA-40 and ERA-Interim (van Angelen et al., 2011). In contrast to the MAR-based reconstructions, this reconstruction is not forced with reanalyses, except for the calibration with RACMO2, but is based on in situ observations (Box, 2013). Absolute uncertainty for the revised SMB estimates from Box (2013) is estimated by comparison against field data. A total of 208 in situ annual ablation rates over 1985–1992 yield an ablation root mean square error of 35 %, similar to the one found with RACMO2.1/GR. The comparison with ice-core-derived net accumulation time series from 86 sites shows a 30 % accumulation RMSE. A fundamental assumption is that the calibration regression factors, derived over 1960–2012 vs. ice cores, from meteorological station temperatures and with RACMO2.1/GR, are stationary in time.

Figure 5c illustrates $MAR_{ERA-Interim}$ SMB validation results. Statistics are listed in Table 3. Correlation exceeds 0.9

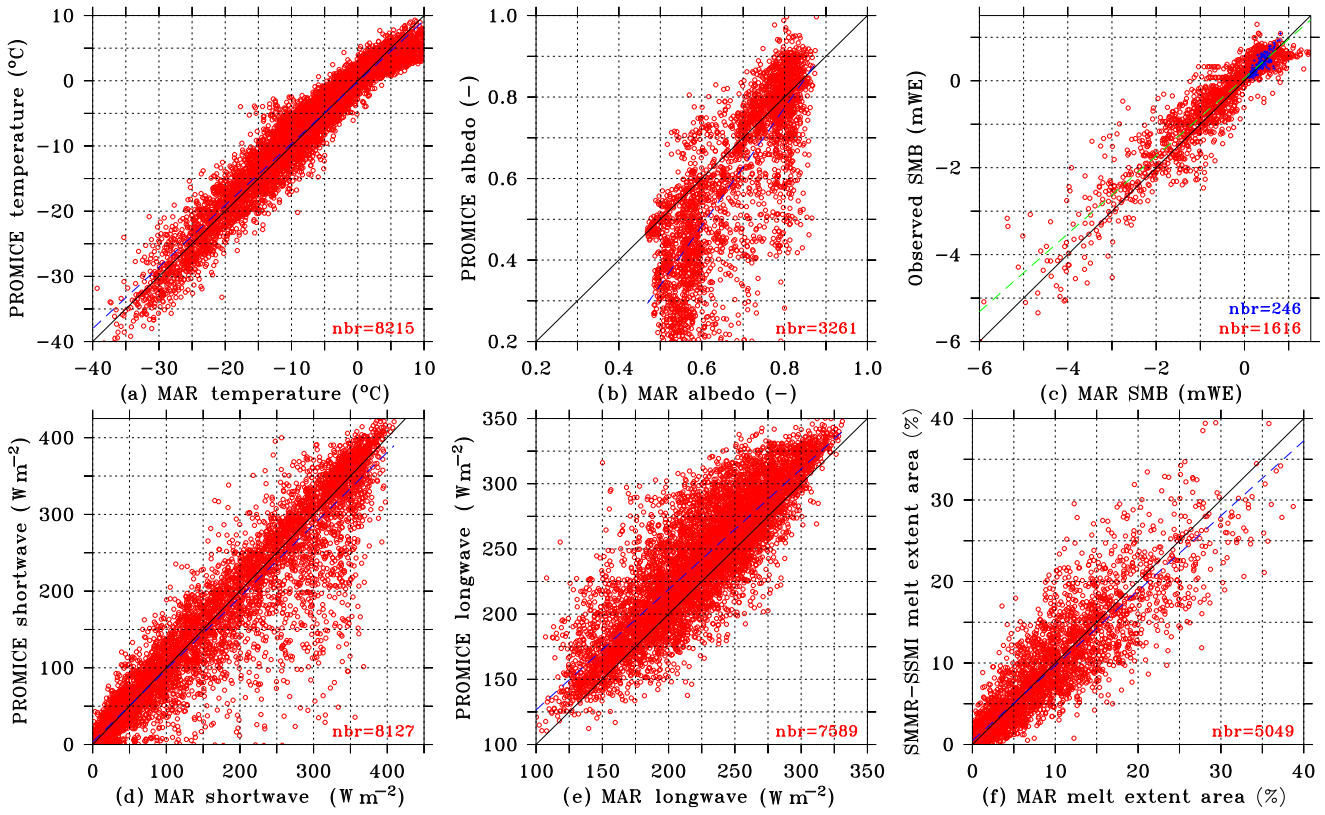

Figure 5. **(a)** Scatter plot of the $MAR_{ERA-Interim}$ daily near-surface temperature vs. near-surface daily temperature recorded by 12 AWSs from the PROMICE network over 2008–2010. The number of observations used here is listed in red and units are °C. **(b)** Same as **(a)** but for the surface albedo. **(c)** Scatter plot of the $MAR_{ERA-Interim}$ SMB (in m w.e.) with respect to ice core measurements in the accumulation area (in blue) and SMB measurements (in red) from the MACHGUTH16 dataset over 1958–2010. We refer to the text for more details on how this comparison is performed. **(d)** Same as **(a)** for the shortwave downward radiative flux (in W m^{-2}). **(e)** Same as **(d)** for the longwave downward radiative flux. **(f)** Daily melt extent (in % of the ice sheet area) simulated by $MAR_{ERA-Interim}$ over the 1979–2010 summers (May–September) vs. the satellite-derived one. More information about the thresholds used for retrieving the melt extent is given in the text.

and RMSE is ∼ 40 % for 1862 samples within the MAR ice sheet mask over 1958–2010. With respect to MARv2, the accumulation overestimation shown by Vernon et al. (2013) has been partly corrected in MARv3.5.2. However, MARv3.5.2 overestimates SMB in the ablation area, while MARv2 underestimates it, as a result of the bare ice albedo overestimation shown in the previous section for MARv3.5.2. The bare ice albedo was fixed to 0.45 in MARv2, while it varies between 0.4 and 0.55 in MARv3.5.2. This shows the impact and importance of improving the bare ice albedo representation in the models, as already stated by van Angelen et al. (2012).

When MAR is forced by reanalyses other than ERA-40 and ERA-Interim, we find that (i) MAR_{NCEPv1} is the most accurate because, over 1958–1978, NCEPv1 is not affected by the humidity bias present in ERA-40 and impacting the MAR precipitation in the non-homogeneous ECMWF time series, (ii) the use of CORR-ERA-20c partially corrects the SMB overestimation (due to the underestimation of melt) obtained when MAR is forced by unadjusted ERA-20C, (iii) MAR_{20CRv2} is more accurate than $MAR_{CORR-20CRv2}$ because the overestimation of melt in MAR_{20CRv2} compensates for the SMB overestimation in the ablation area due to albedo overestimation and (iv) the results of MAR_{NCEPv2} are worse than MAR results using less constrained reanalyses (e.g. 20CRv2) or first generation reanalysis (e.g. NCEPv1), as a result of the temperature biases in NCEPv2. Moreover, while some of these data were used in the Box (2013) reconstruction, the comparison of ice core measurements with BOX13 shows the same agreement with MAR (see Table 3). Regarding the comparison with the SMB MACHGUTH16 database, the SMB values from BOX13 were corrected as a function of the elevation difference with the MACHGUTH16 database as done for MAR. However, to match the exact period of the MACHGUTH16 database, we have simply derived daily values from the monthly BOX13 values by dividing them by the number of days in every month. It is clear that this approximation smoothing the melt variability can be problematic when the period of measurements covers only a few weeks in the melt season and very likely explains why

Table 3. Comparison with SMB from the MACHGUTH16 database over 1958–2010, ice-core-based accumulation from Bales et al. (2001, 2009) and Ohmura et al. (1999), and satellite-derived melt extent over 1979–2010. $MAR_{ERA-Interim}$ (MAR_{ERA-40}) means that MAR was forced by ERA-40 over 1958–1978 (1958–2000) and ERA-Interim over 1979–2015 (2001–2015). Finally, $MAR_{ERA-Interim}{}^{*}$ means that the extrapolation of Franco et al. (2012) was not used to correct the MAR SMB with respect to the elevation differences between MAR and the MACHGUTH16 measurement sites.

Simulation acronym	SMB–MACHGUTH16 (m.w.e.)			Accumulation (m.w.e. yr^{-1})			Melt extent (%)		
	BIAS	RMSE	CORR	BIAS	RMSE	CORR	BIAS	RMSE	CORR
$MAR_{ERA-Interim}$	+0.14	0.46	0.93	+0.02	0.08	0.91	+0.0	2.8	0.93
MAR_{ERA-40}	+0.20	0.48	0.93	+0.03	0.09	0.91	−0.1	2.9	0.92
$MAR_{ERA-20C}$	+0.39	0.67	0.91	−0.03	0.07	0.91	−2.0	3.8	0.90
$MAR_{CORR-ERA-20c}$	+0.22	0.52	0.93	+0.01	0.07	0.91	−0.4	3.0	0.91
MAR_{NCEPv1}	+0.13	0.45	0.93	+0.03	0.09	0.92	+0.2	2.9	0.92
MAR_{NCEPv2}	+0.26	0.52	0.93	+0.03	0.09	0.92	−0.3	2.9	0.92
MAR_{20CRv2}	+0.01	0.47	0.93	+0.01	0.08	0.92	+2.0	4.5	0.92
$MAR_{CORR-20CRv2}$	+0.18	0.50	0.92	+0.01	0.08	0.92	+0.1	3.4	0.91
$MAR_{20CRv2c}$	+0.14	0.49	0.92	+0.02	0.09	0.90	+0.6	3.7	0.91
MAR_{JRA-55}	+0.18	0.48	0.93	+0.01	0.07	0.92	−0.2	2.8	0.92
BOX13	+0.16	0.68	0.84	+0.00	0.08	0.92			
$MARv2_{ERA-Interim}$	−0.08	0.58	0.90	+0.06	0.14	0.82	+0.1	2.9	0.91
$MAR_{ERA-Interim}{}^{*}$	+0.34	0.74	0.86						

BOX13 is less correlated with the MACHGUTH16 dataset than MAR. Finally, it is interesting to note that the comparison with MACHGUTH16 and ice core measurements is quite constant over the entire century (see Table S2) and not better in the recent decades than before despite the larger amount of assimilated data. The lowest correlations are reached in the 1950s and 1960s, but the number of observations is too limited before 1950 to allow for the conclusion that the reliability of the MAR reconstructions are constant in time.

Figure 6 illustrates how MARv3.5.2 still overestimates snow accumulation for the southern ice sheet when compared to ice cores (see Fig. 6b) and BOX13 (see Fig. 6c). However this bias has been partly corrected since MARv2, which was wetter in this area than the current MARv3.5.2 (see Fig. 4a). MAR also underestimates accumulation compared to ice cores in the north-east but is better than the BOX13 results, which are based on RACMO2 and known to underestimate accumulation in this area (Noël et al., 2016). In these areas, the spread in the mean 1958–2010 SMB simulated by MAR using the different reanalyses is below 25 mm.w.e. yr^{-1} (see Fig. 6d), confirming that these biases are independent of the used forcings and that improvements in MAR should improve absolute accuracy. Moreover, these biases are in full agreement with the MAR biases found by Koenig et al. (2016) with respect to 2009–2012 airborne snow-radar-based estimates. In the ablation area (i.e. the MACHGUTH16 sites), the MAR biases vary regionally and no systematic bias can be highlighted. Finally, huge differences ($> 500\,mm\,yr^{-1}$) between MAR and BOX13 occur along the coastal and mountainous regions of the south-east. MAR underestimates accumulation relative to BOX13 (where the latter is based on RACMO2). The Polar MM5 model (24 km) shows the same underestimation with respect to RACMO2 (Box, 2013). Ettema et al. (2009) attributed the higher accumulation rates in these topographically enhanced precipitation regions to the higher spatial resolution used in RACMO2 (11 km). However, a MAR simulation at a resolution of 10 km (not shown here) does not simulate such an extremely high precipitation, and the number of observations in this very wet area is too sparse to confirm the RACMO2-based estimations, suggesting that further accumulation measurement campaigns should focus on this area.

5 Validation with microwave satellite-derived melt extent

As in Fettweis et al. (2011b), we use the brightness temperatures collected at K-band horizontal polarization (T19H) to retrieve the daily melt extent from the scanning multichannel microwave radiometer (SMMR; 1979–1987) and the special sensor microwave/imager (SSM/I; 1988–2010) data distributed by the National Snow and Ice Data Center (NSIDC, Boulder, Colorado; Armstrong et al., 1994; Knowles et al., 2002). A grid cell is considered as melting in MAR (in satellite-based datasets) if the daily meltwater production (T19H) is higher than 8 mm.w.e. yr^{-1} (227.5 K). We refer to Fettweis et al. (2011b) for more details about the melt-retrieving methodology.

As already presented in Fettweis et al. (2011b), the comparison of the melt extent simulated by MAR and retrieved from the passive microwave satellites is encouraging (see

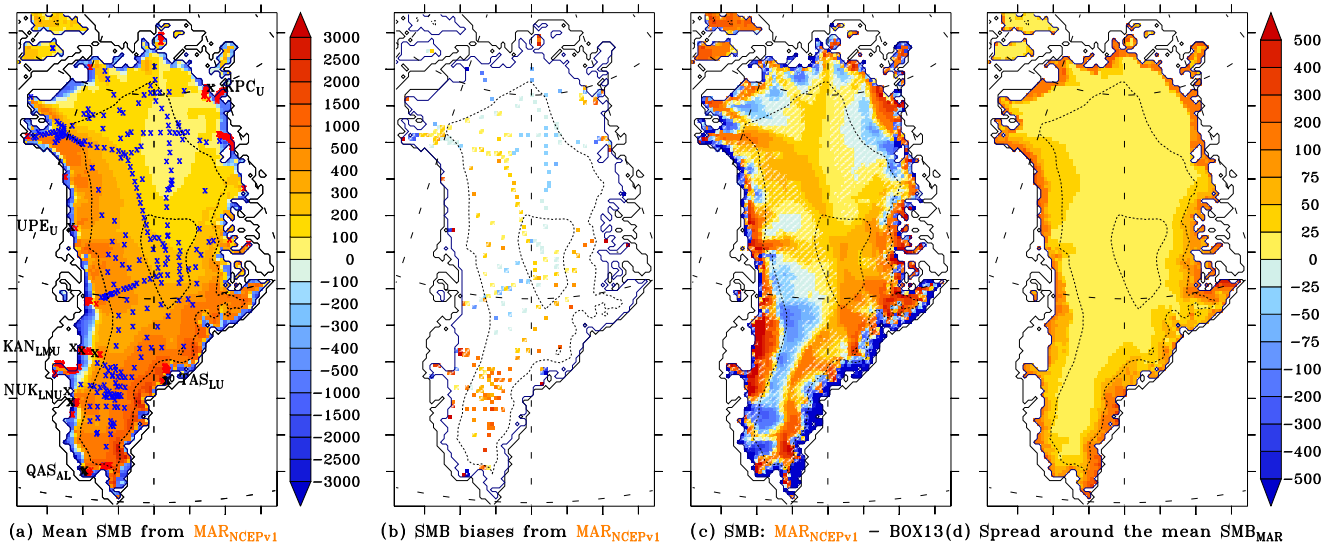

Figure 6. **(a)** Mean annual SMB (in mm.w.e. yr^{-1}) simulated by MAR forced by NCEPv1 over 1958–2010. The ice core locations from Bales et al. (2001, 2009) and Ohmura et al. (1999) used to validate MAR are quoted in blue, while the MACHGUTH16 SMB sites (Machguth et al., 2016) are in red. **(b)** Mean biases (in mm.w.e. yr^{-1}) of MAR forced by NCEPv1 over 1958–2010 with respect to both ice core and MACHGUTH16-based SMB estimations. The biases lower than the interannual variability of MARv3.5.2 forced by NCEPv1 over 1958–2010 are hatched. **(c)** Comparison over 1958–2010 between the mean SMB (in mm.w.e. yr^{-1}) simulated by MAR and from the BOX13 reconstruction. Again, the biases lower than the interannual variability of MARv3.5.2 forced by NCEPv1 over 1958–2010 are hatched. **(d)** Spread (i.e. standard deviation in mm.w.e. yr^{-1}) around 6 estimations of the mean 1958–2010 SMB as simulated by MAR forced by ERA, NCEPv1, JRA, CORR-ERA-20c, CORR-20CRv2 and 20CRv2c.

Table 3 and Fig. 5). The RMSE represents ∼30 % of the daily variability found in the remote-based melt extent over the 1979–2010 summers, and correlations are higher than 0.9, regardless of the forcing used. As already shown in the two previous sections, MAR$_{20CRv2}$ (MAR$_{ERA-20C}$) overestimates (underestimates) the melt extent, fully justifying the corrections applied to 20CRv2 and ERA-20C to reduce these biases. Finally, MARv3.5.2 slightly improves the comparison with respect to MARv2 used in Fettweis et al. (2011b).

6 Time evolution

6.1 Temperature

Figure 7 illustrates MAR's ability to simulate a time series of observed composite near-surface air temperature from Cappelen et al. (2014). As the latter is based on coastal weather station measurements of south and west Greenland, a large part of the interannual variability comes from SST changes, which are prescribed every 6 h into MAR. The remaining part comes from changes in the general circulation (Fettweis et al., 2013a), also prescribed at the MAR lateral boundaries. Therefore, this section evaluates the ability of the different MAR forcings to represent the observed temperature variability. As these observations have been assimilated into BOX13, the latter reconstruction perfectly matches the observations.

The 1900–1920 coastal temperatures were lower than the 1980–2010 average, and their interannual variability, which is only well represented by MAR$_{CORR-20CRv2}$ and MAR$_{20CRv2c}$, is also lower, even though these simulations underestimate the negative temperature anomalies observed during this period according to BOX13. A first maximum of temperature was reached in 1930 and is only well represented by MAR$_{20CRv2c}$. MAR$_{CORR-ERA-20c}$ simulates this maximum earlier while MAR$_{20CRv2c}$ underestimates it. This maximum is also observed in the summer (JJA) time series but underestimated in all of the MAR-based time series. After this optimum warm period discussed in Chylek et al. (2006), there were two minor temperature maxima at the beginning of the 1960s and at the end of the 1970s, which are overestimated by MAR$_{20CRv2c}$ and MAR$_{NCEPv1}$ and underestimated by the MAR time series using the other forcings. Temperature differences of several degrees between the JRA-forced time series before and during the satellite era (starting at the end of the 1970s) suggest biases in the JRA-based SST before 1980. Except in MAR$_{CORR-20CRv2}$ (and to a lesser extent in MAR$_{ERA-Interim}$), where the temperature variability is very smooth, the summer and annual warming in the 1990s and 2000s is well represented in all of the MAR-based times series.

When integrated over the entire ice sheet (see Fig. 7c), all MAR reconstructions show a decrease of the summer mean temperature (gauging the melt) after 1930 until the begin-

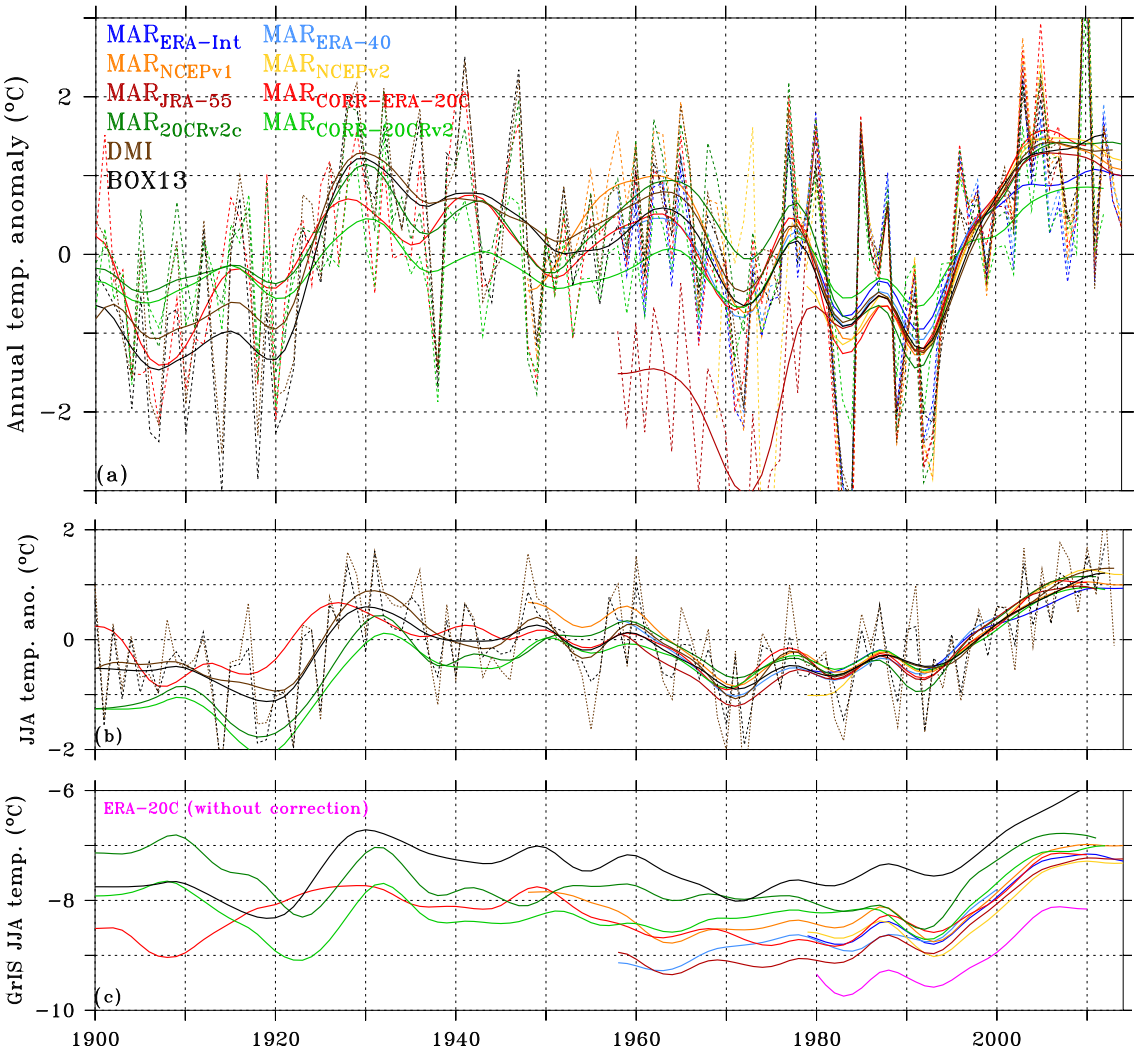

Figure 7. (a) Time series of the annual SW Greenland near-surface temperature (built by merging series of the Ilulissat, Nuuk and Qaqortoq coastal weather stations from the Danish Meteorological Institute,DMI) as observed (in brown) according to Cappelen et al. (2014), retrieved from the BOX13 reconstruction (in black) and as simulated by MAR with the different forcings. Values are anomalies with respect to 1980–2010 and 10-year running mean are shown. **(b)** Same as **(a)** for the summer (JJA) SW Greenland near-surface temperature. **(c)** Mean GrIS summer (JJA) near-surface temperature (in °C) as simulated by MAR using the different forcings. The ERA-20c (without temperature correction) forced MAR time series as well as the BOX13 reconstruction-based time series are also shown.

ning of the 1990s, when an abrupt temperature increase of $\sim 2\,^{\circ}C$ in 10 years is simulated. Before 1930, the MAR reconstructions diverge even though the reanalyses are supposed to represent the same climate variability. However, the comparison with BOX13 constrained by DMI coastal weather station measurements is the closest when MAR is forced by (CORR-)20CRv2(c) because SST is assimilated into 20CRv2(c) but not into ERA-20C. Finally, as absolute temperatures are shown here, we can see that MAR is systematically 0.5–1 °C colder than BOX13 as a result of the MAR cold bias discussed in Sect. 4.1.

6.2 Surface mass balance

Time series of the SMB components integrated over the whole GrIS are presented in Fig. 8. Before 1930, as for the JJA mean GrIS near-surface temperature (see Fig. 7), there are large discrepancies between the MAR-based run-off reconstructions, suggesting that large improvements (i.e. assimilating more data) are still needed in the reanalysis before this period. After the warm period observed in the 1930s (Chylek et al., 2006), all of the MAR reconstructions suggest an increasing SMB due to heavier snowfall and lower melt. Regarding the period 1960–1990, the meltwater run-off amount is low and stable. The highest SMB occurred in the

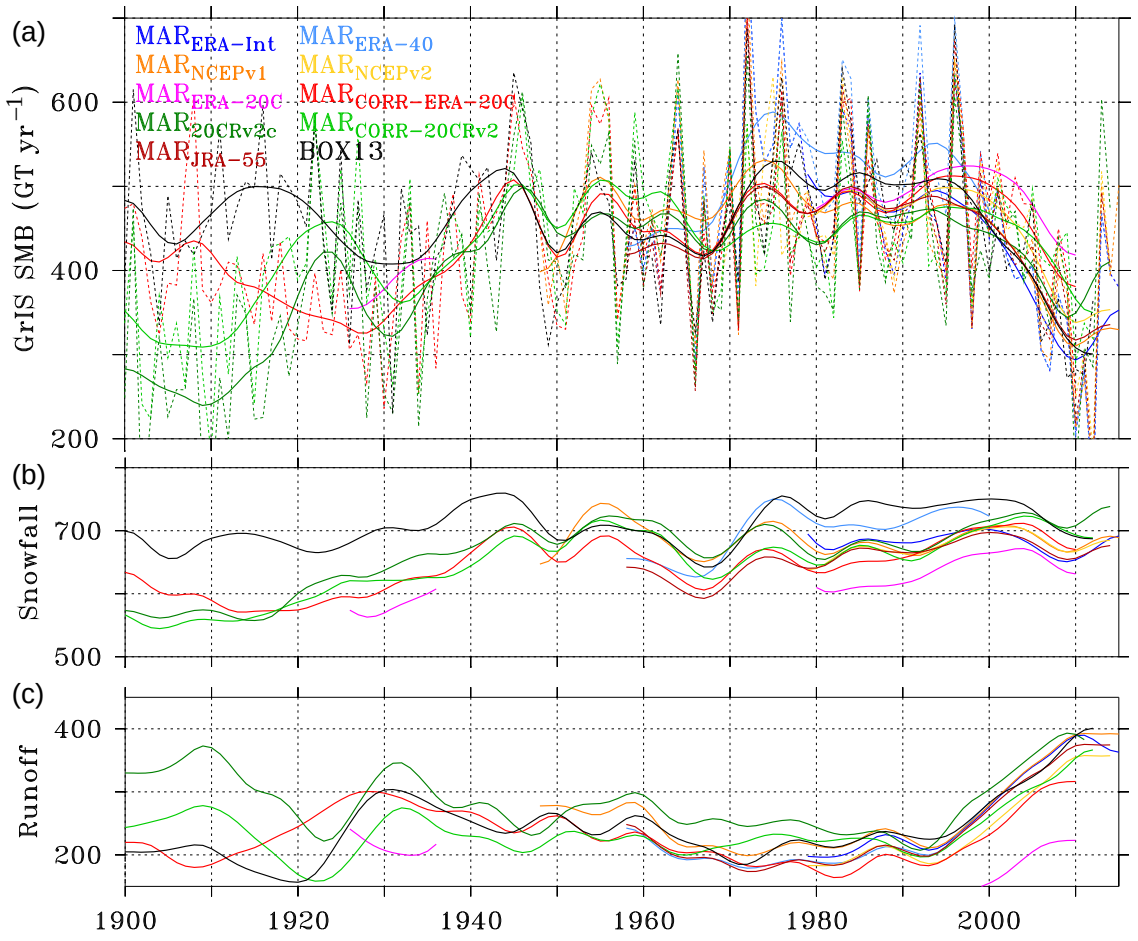

Figure 8. **(a)** Time series of the annual SMB (in GT yr^{-1}) integrated over the whole ice sheet as simulated by MAR using the different listed forcings and coming from Box's reconstruction (BOX13). **(b)** Same as **(a)** but for snowfall. **(c)** Same as **(a)** but for run-off. Finally, only 10-year running means are shown for both **(b)** and **(c)** for more readability.

1970s, but there are some discrepancies among the models. This maximum is the highest when MAR is forced by ERA-40, which is also used to force RACMO, on which BOX13 is based. At the beginning of this century, all the models simulate an SMB decrease that reaches a record minimum in or after 2010, resulting from an increasing surface melt. A second SMB minimum is simulated around 1930 by MAR as a result of high melt and low accumulation. This minimum is less pronounced in BOX13 because it includes considerable smoothing by the weighted averaging of annual core and monthly station temperature values. Therefore, BOX13 may suffer from more damping than what MAR can produce with 6-hourly forcings. Finally, MAR suggests a significant snowfall increase from 1900–1920 to 1950, in opposition to Hanna et al. (2011). However, such an increase is also suggested in the (Box et al., 2013) reconstruction and in the ice cores (Mernild et al., 2015) but is less pronounced than in the MAR simulations (see Fig. 9). Part of the MAR-simulated snowfall increase may be caused by an artificial increase of the daily sea level pressure variability over 1900–1950 (see Fig. 9d) and the associated strengthened eddy activity. The 20CRv2c reanalysis is an ensemble mean, suggesting that the lower the amount of assimilated data is, the higher the spread is for a given event. This smooths the pressure fields and therefore decreases the amount of humidity advected into the MAR free atmosphere and subsequently the precipitation rate simulated by MAR, even if the 20CRv2 reanalysis itself simulates higher precipitation during this period (Hanna et al., 2011). ERA-20C is not an ensemble mean but it is likely that a lower amount of assimilated data also induce smoother pressure fields. However, ERA-20C seems to suggest that the storm activity was higher at the beginning of the last century than in the 1920–1940 period. Therefore, this apparent significant precipitation increase from 500 to > 600 Gt yr^{-1} simulated by MAR over 1900–1950 should be considered with caution since both reanalyses-forced MAR simulations disagree on the location where this increase takes place (western coast vs. eastern coast) and whether a part of this increase could just be due to an artefact in the 20CRv2(c). Finally, it is interesting to

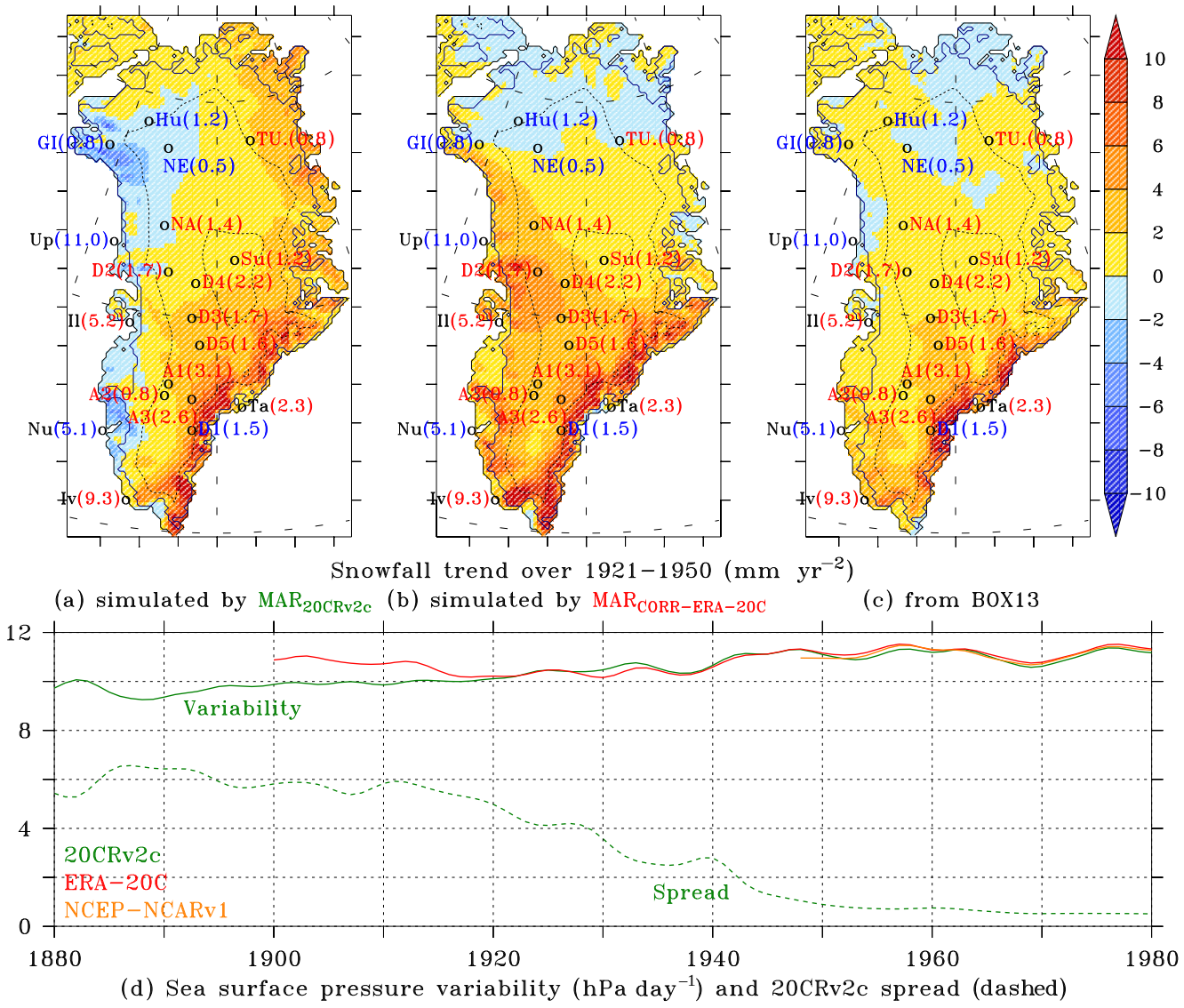

Figure 9. **(a)** Annual snowfall trend (in mm.w.e. yr^{-2}) over 1921–1950 as simulated by MAR forced by 20CRv2c. The observed trend (in mm.w.e. yr^{-2}) from some locations listed in Mernild et al. (2015) are also highlighted on the figure. These observed negative (positive) trends are the values printed in blue (in red) on the map. Trends of total precipitation (rain + snow) are also labelled in black for five coastal weather stations from DMI. **(b)** Same as **(a)** but for MAR$_{CORR-ERA-20c}$. **(c)** Same as **(a)** but for BOX13. **(d)** Time series of the annual mean daily variability (i.e. standard deviation of the daily values) of the sea level pressure around Greenland (0° W ≤ longitude ≤ 80° W and 55° N ≤ latitude ≤ 85° N) from 20CRv2c (in green), ERA-20C (in red) and NCEPv1 (in orange). The ensemble mean spread (i.e. the standard deviation of the ensemble deviations at each time) from 20CRv2c over the same area is also plotted with dashes. Finally, only 10-year running means are shown for more readability.

note that (Hanna et al., 2016) also showed an increase of the variability of the 20CRv2c-based Greenland blocking index through the last century.

We can see in Fig. 9 that the pattern of snowfall increase over 1921–1950 is quite different following the reconstruction and that there are some disagreements with the ice-core-based trend listed in Mernild et al. (2015). MAR$_{20CRV2c}$ suggests a decrease of accumulation along the west coast and a significant increase along the eastern coast with the highest increase at the south-east, as the other reconstructions. MAR$_{CORR-ERA-20c}$ suggests a decrease only at the north of the ice sheet and a significant increase along the western coast, in disagreement with the two other reconstructions. Finally, BOX13 suggests an increase only at the south (south-east) of the ice sheet. The decrease seen in the ice cores in the Humboldt–NEEM area (at the north-west) is well represented by the three reconstructions, but they fail to simulate the decrease observed at D1 near Tasiilaq. The other

ice cores rather suggests a positive trend in agreement with all the reconstructions, but MAR mostly overestimates the observed trend, while BOX13 is in better agreement with ice cores. The significant accumulation increase simulated by $MAR_{20CRV2c}$ along the north-eastern coast and simulated by $MAR_{CORR-ERA-20c}$ along the western coast seems to be overestimated with respect to ice core measurements. Unfortunately, no gauge observation is available along the south-eastern coast to confirm the significant snowfall increase simulated by the three reconstructions in this area over 1921–1950.

7 Discussion and conclusions

Reconstructions of the GrIS SMB from the beginning of the last century (1900–2015) were carried out using the regional climate MAR model forced by eight reanalyses. Over the recent decades, all MAR time series compare very well with in situ measurements, ice core and satellite-derived melt extent, while temperature corrections were needed in the 20CRv2 and ERA-20C reanalyses at the MAR boundaries. MAR forced by ERA-Interim shows the best comparison with observations for 1979 onward, while NCEP–NCARv1 outperforms ERA-40 and JRA-55 over 1958–1978. Among the reanalyses covering the entire century, 20CRv2c is the only reanalysis that does not need correction at the MAR boundaries, but its performance is not as good as the fully assimilated reanalyses such as ERA-Interim over the recent decades.

Around 1930, all reconstructions agree on an SMB minimum concurrent with the warm period observed in the coastal temperatures (Chylek et al., 2006). Afterwards, the reconstructions suggest a melt decrease until the 1970s and an accumulation increase until the middle of the 1940s. A second minimum of SMB occurs in the 1960s when a minimum of accumulation is reached, while the highest SMB rates are reached over the 1970s–early 1990s, as a consequence of lower melt and higher accumulation than before. All reconstructions then show a significant SMB decrease resulting from a surface melt increase starting at the end of the 1990s and lasting until the 2010s, when the SMB absolute minimum since 1900 is reached in all time series.

Before the 1930s, there are, however, large discrepancies between the MAR reconstructions as well as with the Box (2013) time series. MAR forced by ERA-20C suggests a continuous run-off increase from the 1900s to 1930s, while MAR forced by 20CRv2(c) and, to a lesser extent, BOX13 suggests a run-off decrease from the 1900s until the 1910s, followed by a melt increase reaching a first maximum at the beginning of the 1930s. Similar discrepancies can be seen in the MAR-simulated near-surface temperatures. MAR also simulates a significant snowfall increase from the 1910s to the 1940s. Reconstructions from Box et al. (2013) and ice cores (Mernild et al., 2015) also suggest an accumulation increase over this period but smaller than MAR's increase, while Hanna et al. (2011) suggested a decrease of the accumulation. Long-term ice core data facilitate validation of an overall ice sheet snowfall increase in the first half of the last century, and the comparison with MAR is good where a few ice cores are available. This increase is, however, bracketed in several ice cores in the dry north as well simulated by MAR, but not for the only core (see D1 in Fig. 9) in the south-east showing decreasing snowfall. Thus, the ice sheet-averaged core trend is almost insignificant, while MAR suggests a significant increase along the south-east coastal ridge where ice cores are missing. This suggests that new ice core drillings are needed in this area to confirm the MAR accumulation increase. Moreover, this accumulation increase in MAR coincides with an increase of the daily sea level pressure variability in forcing reanalyses, which impacts the amount of humidity advected into the MAR integration domain. The 20CRv2(c) reanalysis is an ensemble mean of 56 members, suggesting that the lower the amount of assimilated data is, the smoother the pressure fields are. Therefore, the increase of the daily sea level pressure variability could just be an artefact coming from forcing reanalysis. While ERA-20C is not an ensemble mean, MAR forced by this reanalysis shows the same magnitude of precipitation increase as MAR forced by 20CRv2(c), but not at the same locations. On the other hand, the amount of data assimilated into ERA-20C is lower during this period. Therefore, without gauge observations in the areas where the changes are the highest, it is hard to conclude whether this MAR-based significant accumulation increase along the south-east coastal ridge over the first half of the last century is robust or whether it is just an artefact coming from the forcing reanalyses (which need to be more constrained to be in agreement before the 1930s). Belleflamme et al. (2013) already showed large discrepancies in the general circulation simulated over Greenland by these two reanalyses before 1940, explaining the significant differences in the simulated run-off and snowfall variability.

The period 1961–1990 has been considered as a period when the total mass balance of the Greenland ice sheet was stable (Rignot and Kanagaratnam, 2006) and near zero. However, at the last century scale, all MAR reconstructions suggest that SMB was particularly positive during this period (SMB was most positive from the 1970s to the middle of the 1990s), suggesting that mass gain may well have occurred during this period, in agreement with results from Colgan et al. (2015).

Finally, with respect to the 1961–1990 period, the integrated contribution of the GrIS SMB anomalies over 1900–2010 is a sea level rise of about 15 ± 5 mm, with a null contribution from the 1940s to the 2000s, suggesting that the recent contribution of GrIS to sea level change (van den Broeke et al., 2016) is unprecedented in the last century. A next step to evaluate total mass changes should be to force ice sheet models with these MAR reconstructions to confirm the stability of the ice dynamics over 1961–1990 and to better un-

derstand the recent acceleration of ice dynamics (van den Broeke et al., 2016). This recent acceleration of ice dynamics could partly result from the purge of the extra mass (accumulated through the 1970–1990s) enhanced by the recent melt increase lubricating the glaciers–bedrock interface.

Data availability. All MARv3.5.2 outputs presented here are available at ftp://ftp.climato.be/fettweis/MARv3.5/Greenland/, and the source code of MARv3.5.2 is available at ftp://ftp.climato.be/fettweis/MARv3.5/.src/. The ECMWF reanalyses (ERA-Interim, ERA-40 and ERA-20C) were downloaded from http://apps.ecmwf.int/datasets/. The NCEP–NCARv1, NCEP–NCARv2 and the 20CRv2(c) reanalyses come from http://www.esrl.noaa.gov/psd/data/, while the JRA-55 reanalysis comes from https://climatedataguide.ucar.edu/climate-data. The brightness temperatures used to retrieve the melt extent from the satellite were downloaded from http://nsidc.org/. Finally, the PROMICE and MACHGUTH16 data used to validate MAR are available at http://www.promice.dk/.

The Supplement related to this article is available online at doi:10.5194/tc-11-1015-2017-supplement.

Competing interests. The authors declare that they have no conflict of interest.

Acknowledgements. The PROMICE (Programme for Monitoring of the Greenland Ice Sheet) network is funded by the Danish Energy Agency (DANCEA) programme. Computational resources have been provided by the Consortium des Équipements de Calcul Intensif (CÉCI), funded by the Fonds de la Recherche Scientifique de Belgique (F.R.S.–FNRS) under grant no. 2.5020.11 and the Tier-1 supercomputer (Zenobe) of the Fédération Wallonie-Bruxelles infrastructure funded by the Walloon Region under the grant agreement no. 1117545. Finally, X. Fettweis is a Research Associate from the Fonds de la Recherche Scientifique de Belgique (F.R.S.-FNRS), and J. Box was supported by the Danish Research Council grant FNU 4002-00234.

Edited by: E. Hanna
Reviewed by: E. Hanna and one anonymous referee

References

Ahlstrom, A. P., Gravesen, P., Andersen, S. B., Van As, D., Citterio, M., Fausto, R. S., Nielsen, S., Jepsen, H. F., Kristensen, S. S., Christensen, E. L., Stenseng, L., Forsberg, R., Hanson, S., Petersen, D., and PROMICE Project Team: A new programme for monitoring the mass loss of the Greenland ice sheet, Geol. Surv. Den. Green. Bull., 15, 61–64, 2008.

Alexander, P. M., Tedesco, M., Fettweis, X., van de Wal, R. S. W., Smeets, C. J. P. P., and van den Broeke, M. R.: Assessing spatio-temporal variability and trends in modelled and measured Greenland Ice Sheet albedo (2000–2013), The Cryosphere, 8, 2293–2312, doi:10.5194/tc-8-2293-2014, 2014.

Alexander, P. M., Tedesco, M., Schlegel, N.-J., Luthcke, S. B., Fettweis, X., and Larour, E.: Greenland Ice Sheet seasonal and spatial mass variability from model simulations and GRACE (2003–2012), The Cryosphere, 10, 1259–1277, doi:10.5194/tc-10-1259-2016, 2016.

Armstrong, R. L., Knowles, K. W., Brodzik, M. J., and Hardman M. A.: DMSP SSM/I Pathfinder daily EASE-Grid brightness temperatures, May 1987 to April 2009, Boulder, CO, USA, National Snow and Ice Data Center, Digital media and CD-ROM, 1994.

Bamber, J. L., Layberry, R. L., and Gogenini, S. P.: A new ice thickness and bed dataset for the Greenland ice sheet 1: measurement, data reduction, and errors, J. Geophys. Res., 106, 33773–33780, 2001.

Bales, R. C., McConnell, J. R., Mosley-Thompson, R., and Csatho, B.: Accumulation over the Greenland ice sheet from historical and recent records, J. Geophys. Res., 106, 33813–33825, doi:10.1029/2001JD900153, 2001.

Bales, R. C., Guo, Q., Shen, D., McConnell, J. R., Du, G., Burkhart, J. F., Spikes, V. B., Hanna, E., and Cappelen, J.: Annual accumulation for Greenland updated using ice core data developed during 2000–2006 and analysis of daily coastal meteorological data, J. Geophys. Res., 114, D06116, doi:10.1029/2008JD011208, 2009.

Bamber, J. L., Griggs, J. A., Hurkmans, R. T. W. L., Dowdeswell, J. A., Gogineni, S. P., Howat, I., Mouginot, J., Paden, J., Palmer, S., Rignot, E., and Steinhage, D.: A new bed elevation dataset for Greenland, The Cryosphere, 7, 499–510, doi:10.5194/tc-7-499-2013, 2013.

Belleflamme, A., Fettweis, X., and Erpicum, M.: Recent summer Arctic atmospheric circulation anomalies in a historical perspective, The Cryosphere, 9, 53–64, doi:10.5194/tc-9-53-2015, 2015.

Box, J. E.: Greenland ice sheet mass balance reconstruction, Part II: Surface mass balance (1840–2010), J. Climate, 26, 6974–6989, doi:10.1175/JCLI-D-12-00518.1, 2013.

Box, J. E., Cressie, N., Bromwich, D. H., Jung, J., van den Broeke, M., van Angelen, J. H., Forster, R. R., Miège, C., Mosley-Thompson, E., Vinther, B., and McConnell, J. R.: Greenland ice sheet mass balance reconstruction, Part I: net snow accumulation (1600–2009), J. Climate, 26, 3919–3934, doi:10.1175/JCLI-D-12-00373.1, 2013.

Brun, E., David, P., Sudul, M., and Brunot, G.: A numerical model to simulate snowcover stratigraphy for operational avalanche forecasting, J. Glaciol., 38, 13–22, 1992.

Cappelen, J. and Vinther B. M.: SW Greenland temperature data 1784-2013, DMI Technical Report 14-06, Copenhagen, 2014.

Chylek, P., Dubey, M. K., and Lesins, G.: Greenland warming of 1920–1930 and 1995–2005, Geophys. Res. Lett., 33, L11707, doi:10.1029/2006GL026510, 2006.

Colgan, W., Box, J., Andersen, M., Fettweis, X., Csatho, B., Fausto, R., van As, D., and Wahr J.: Greenland high elevation mass balance: inference and implication of reference period (1961–90) imbalance, Ann. Glaciol., 56, 105–117, doi:10.3189/2015AoG70A967, 2015.

Compo, G. P., Whitaker, J. S., Sardeshmukh, P. D., Matsui, N., Allan, R. J., Yin, X., Gleason, B. E., Vose, R. S., Rutledge, G., Bessemoulin, P., Brönnimann, S., Brunet, M., Crouthamel, R. I., Grant, A. N., Groisman, P. Y., Jones, P. D., Kruk, M., Kruger, A.

C., Marshall, G. J., Maugeri, M., Mok, H.Y., Nordli, Ø., Ross, T. F., Trigo, R. M., Wang, X. L., Woodruff, S. D., and Worley, S. J.: The Twentieth Century Reanalysis Project, Q. J. Roy. Meteorol. Soc., 137, 1–28, doi:10.1002/qj.776, 2011.

Cullather R. I., Nowicki, S. M. J., Zhao, B., and Koenig, L. S.: A Characterization of Greenland Ice Sheet Surface Melt and Runoff in Contemporary Reanalyses and a Regional Climate Model, Front. Earth Sci., 4, 10 pp., doi:10.3389/feart.2016.00010, 2016.

Dee, D. P., Uppala, S. M., Simmons, A. J., Berrisford, P., Poli, P., Kobayashi, S., Andrae, U., Balmaseda, M. A., Balsamo, G., Bauer, P., Bechtold, P., Beljaars, A. C. M., van de Berg, I., Biblot, J., Bormann, N., Delsol, C., Dragani, R., Fuentes, M., Greer, A. J., Haimberger, L., Healy, S. B., Hersbach, H., Holm, E. V., Isaksen, L., Kallberg, P., Kohler, M., Matricardi, M., McNally, A. P., Mong-Sanz, B. M., Morcette, J.-J., Park, B.-K., Peubey, C., de Rosnay, P., Tavolato, C., Thepaut, J. N., and Vitart, F.: The ERA-Interim reanalysis: Configuration and performance of the data assimilation system, Q. J. Roy. Meteorol. Soc., 137, 553–597, 2011.

Ettema, J., van den Broeke, M. R., van Meijgaard, E., van de Berg, W. J., Bamber, J. L., Box, J. E., and Bales, R. C.: Higher surface mass balance of the Greenland ice sheet revealed by high-resolution climate modeling, Geophys. Res. Lett., 36, L12501, doi:10.1029/2009GL038110, 2009.

Fettweis, X.: Reconstruction of the 1979–2006 Greenland ice sheet surface mass balance using the regional climate model MAR, The Cryosphere, 1, 21-40, doi:10.5194/tc-1-21-2007, 2007.

Fettweis, X., Hanna, E., Gallée, H., Huybrechts, P., and Erpicum, M.: Estimation of the Greenland ice sheet surface mass balance for the 20th and 21st centuries, The Cryosphere, 2, 117–129, doi:10.5194/tc-2-117-2008, 2008.

Fettweis, X., Tedesco, M., van den Broeke, M., and Ettema, J.: Melting trends over the Greenland ice sheet (1958–2009) from spaceborne microwave data and regional climate models, The Cryosphere, 5, 359–375, doi:10.5194/tc-5-359-2011, 2011.

Fettweis, X., Hanna, E., Lang, C., Belleflamme, A., Erpicum, M., and Gallée, H.: Brief communication "Important role of the mid-tropospheric atmospheric circulation in the recent surface melt increase over the Greenland ice sheet", The Cryosphere, 7, 241-248, doi:10.5194/tc-7-241-2013, 2013a.

Fettweis, X., Franco, B., Tedesco, M., van Angelen, J. H., Lenaerts, J. T. M., van den Broeke, M. R., and Gallée, H.: Estimating the Greenland ice sheet surface mass balance contribution to future sea level rise using the regional atmospheric climate model MAR, The Cryosphere, 7, 469–489, doi:10.5194/tc-7-469-2013, 2013b.

de Fleurian, B., Morlighem, M., Seroussi, H., Rignot, E., van den Broecke, M. R., Kuipers Munneke, P., Mouginot, J., Smeets, C. J. P. P., and Tedstone, A. J.: A modeling study of the effect of runoff variability on the effective pressure beneath Russell Glacier, West Greenland, J. Geophys. Res.-Earth, 121, 1834–1848, doi:10.1002/2016JF003842, 2016.

Franco, B., Fettweis, X., Lang, C., and Erpicum, M.: Impact of spatial resolution on the modelling of the Greenland ice sheet surface mass balance between 1990–2010, using the regional climate model MAR, The Cryosphere, 6, 695–711, doi:10.5194/tc-6-695-2012, 2012.

Hanna, E., Huybrechts, P., Cappelen, J., Steffen, K., Bales, R., Burgess, E., McConnell, J., Steffensen, J. P., Van den Broeke, M., Wake, L., Bigg, B., Griffiths, M., and Savas, D.: Greenland Ice Sheet surface mass balance 1870 to 2010 based on Twentieth Century Reanalysis, and links with global climate forcing, J. Geophys. Res., 116, D24121, doi:10.1029/2011JD016387, 2011.

Hanna, E., Cropper, T. E., Hall, R. J., and Cappelen, J.: Greenland Blocking Index 1851–2015: a regional climate change signal, Int. J. Climatol., 36, 4847–4861, doi:10.1002/joc.4673, 2016.

Kalnay, E., Kanamitsu, M., Kistler, R., Collins, W., Deaven, D., Gandin, L., Iredell, M., Saha, S., White, G., Woollen, J., Zhu, Y., Leetmaa, A., Reynolds, B., Chelliah, M., Ebisuzaki, W., Higgins, W., Janowiak, J., Mo, K., Ropelewski, C., Wang, J., Jenne, R., and Joseph, D.: The NCEP-NCAR 40 year reanalysis project, B. Am. Meteorol. Soc., 77, 437–471, 1996.

Kanamitsu, M., Ebisuzaki, W., Woollen, J., Yang, S.-K., Hnilo, J. J., Fiorino, M., and Potter, G. L.: NCEP–DOE AMIP-II Reanalysis (R-2), B. Am. Meteorol. Soc., 83, 1631–1643, doi:10.1175/BAMS-83-11-1631, 2002.

Kjeldsen, K. K., Korsgaard, N. J., Bjørk, A. A., Khan, S. A., Box, J. E., Funder, S., Larsen, N. K., Bamber, J. L., Colgan, W., van den Broeke, M., Siggad-Andersen, M. L., Nuth, C., Schomacker, A., Andresen, C. S., Willerslev, W., and Kjær, K. H.: Spatial and temporal distribution of mass loss from the Greenland Ice Sheet since AD 1900, Nature, 528, 396–400, doi:10.1038/nature16183, 2015.

Kobayashi, S., Ota, Y., Harada, Y., Ebita, A., Moriya, M., Onoda, H., Onogi, K., Kamahori, H., Kobayashi, C., Endo, H., Miyaoka, K., and Takahashi, K.: The JRA-55 Reanalysis: General Specifications and Basic Characteristics, J. Meteorol. Soc. Jpn., 93, 5–48, doi:10.2151/jmsj.2015-001, 2015.

Koenig, L. S., Ivanoff, A., Alexander, P. M., MacGregor, J. A., Fettweis, X., Panzer, B., Paden, J. D., Forster, R. R., Das, I., McConnell, J. R., Tedesco, M., Leuschen, C., and Gogineni, P.: Annual Greenland accumulation rates (2009–2012) from airborne snow radar, The Cryosphere, 10, 1739–1752, doi:10.5194/tc-10-1739-2016, 2016.

Knowles, K., Njoku, E., Armstrong, R., and Brodzik, M. J.: Nimbus-7 SMMR Pathfinder Daily EASE-Grid Brightness Temperatures, Natl. Snow Ice Data Center, Boulder, Colorado, 2002.

Lucas-Picher, P., Wulff-Nielsen, M., Christensen, J. H., Adalgeirsdottir, G., Mottram, R., and Simonsen, S. B.: Very high resolution regional climate model simulations over Greenland: Identifying added value, J. Geophys. Res., 117, D02108, doi:10.1029/2011JD016267, 2012.

Machguth, H., Thomsen, H. H., Weidick, A., Abermann, J., Ahlström, A. P., Andersen, M. L., Andersen, S. B., Björk, A. A., Box, J. E., Braithwaite, R. J., Bøggild, C. E., Citterio, M., Clement, P., Colgan, W., Fausto, R. S., Gleie, K., Hasholt, B., Hynek, B., Knudsen, N. T., Larsen, S. H., Mernild, S., Oerlemans, J., Oerter, H., Olesen, O. B., Smeets, C. J. P. P., Steffen, K., Stober, M., Sugiyama, S., van As, D., van den Broeke, M. R., and van de Wal, R. S.: Greenland surface mass balance observations from the ice sheet ablation area and local glaciers, J. Glaciol., 62, 861–887, doi:10.1017/jog.2016.75, 2016.

Mernild, S. H. and Liston G. E.: Greenland Freshwater Runoff, Part II: Distribution and Trends, 1960–2010, J. Climate, 25, 6015–6035, doi:10.1175/JCLI-D-11-00592.1, 2013.

Mernild, S. H., Hanna, E., McConnell, J. R., Sigl, M., Beckerman, A. P., Yde, J. C., Cappelen, J., Malmros, J. K., and Steffen, K.: Greenland precipitation trends in a long-term instrumental cli-

mate context (1890–2012): evaluation of coastal and ice core records, Int. J. Climatol., 35, 303–320, doi:10.1002/joc.3986, 2015.

Noël, B., van de Berg, W. J., Machguth, H., Lhermitte, S., Howat, I., Fettweis, X., and van den Broeke, M. R.: A daily, 1 km resolution data set of downscaled Greenland ice sheet surface mass balance (1958–2015), The Cryosphere, 10, 2361–2377, doi:10.5194/tc-10-2361-2016, 2016.

Ohmura, A., Calanca, P., Wild, M., and Anklin M.: Precipitation, accumulation and mass balance of the Greenland Ice sheet, Z. Gletscherkd. Glazialgeol., 35, 1–20, 1999.

Pfeffer, W. T., Meier, M. F., and Illangasekare, T. H. Retention of Greenland runoff by refreezing: implications for projected future sea level change, J. Geophys. Res., 96, 22117–22124, 1991.

Poli, P., Hersbach, H., Dee, D. P., Berrisford, P., Simmons, A. J., Vitart, F., Laloyaux, P., Tan, D. G. H., Peubey, C., Thepaut, J., Tremolet, Y, Holm, E. V., Bonavita, M., Isaksen, L., and Fisher, M.: ERA-20C: An Atmospheric Reanalysis of the Twentieth Century, J. Climate, doi:10.1175/JCLI-D-15-0556.1, 2016.

Rae, J. G. L., Adalgeirsdóttir, G., Edwards, T. L., Fettweis, X., Gregory, J. M., Hewitt, H. T., Lowe, J. A., Lucas-Picher, P., Mottram, R. H., Payne, A. J., Ridley, J. K., Shannon, S. R., van de Berg, W. J., van de Wal, R. S. W., and van den Broeke, M. R.: Greenland ice sheet surface mass balance: evaluating simulations and making projections with regional climate models, The Cryosphere, 6, 1275–1294, doi:10.5194/tc-6-1275-2012, 2012.

Reijmer, C. H., van den Broeke, M. R., Fettweis, X., Ettema, J., and Stap, L. B.: Refreezing on the Greenland ice sheet: a comparison of parameterizations, The Cryosphere, 6, 743–762, doi:10.5194/tc-6-743-2012, 2012.

Rignot, E. and Kanagaratnam, P.: Changes in the Velocity Structure of the Greenland Ice Sheet, Science, 311, 986–990, doi:10.1126/science.1121381, 2006.

Serreze, M. C. and R. G. Barry. Processes and impacts of Arctic amplification: A research synthesis, Global Planet. Change, 77, 85–96, doi:10.1016/j.gloplacha.2011.03.004, 2011.

Sundal, A. V., Shepherd, A., Nienow, P., Hanna, E., Palmer, S., and Huybrechts, P.: Melt-induced speed-up of Greenland ice sheet offset by efficient subglacial drainage, Nature, 469, 521–524, doi:10.1038/nature09740, 2011.

Tedesco, M., Doherty, S., Fettweis, X., Alexander, P., Jeyaratnam, J., and Stroeve, J.: The darkening of the Greenland ice sheet: trends, drivers, and projections (1981–2100), The Cryosphere, 10, 477–496, doi:10.5194/tc-10-477-2016, 2016.

Tedstone, A. J., Nienow, P. W., Sole, A. J., Mair, D. W., Cowton, T. R., Bartholomew, I. D., and King, M. A.: Greenland ice sheet motion insensitive to exceptional meltwater forcing, P. Natl. Acad. Sci. USA, 110, 19719–19724, doi:10.1073/pnas.1315843110, 2013.

Uppala, S. M., Kållberg, P. W., Simmons, A. J., Andrae, U., Da Costa Bechtold, V., Fiorino, M., Gibson, J.K., Haseler, J., Hernandez, A., Kelly, G. A., Li, X., Onogi, K., Saarinen, S., Sokka, N., Allan, R. P., Anderson, E., Arpe, K., Balmaseda, M. A., Beljaars, A. C. M., Van De Berg, L., Bidlot, J., Bormann, N., Caires, S., Chevallier, F., Dethof, A., Dragosavac, M., Fisher, M., Fuentes, M., Hagemann, S., Hólm, E., Hoskins, B. J., Isaksen, L., Janssen, P. A. E. M., Jenne, R., Mcnally, A. P., Mahfouf, J.-F., Morcrette, J.-J., Rayner, N. A., Saunders, R. W., Simon, P., Sterl, A., Trenbreth, K. E., Untch, A., Vasiljevic, D., Viterbo, P., and Woollen, J.: The ERA-40 re-analysis, Q. J. Roy. Meteor. Soc., 131, 2961–3012, doi:10.1256/qj.04.176, 2005.

Schlegel, N.-J., Wiese, D. N., Larour, E. Y., Watkins, M. M., Box, J. E., Fettweis, X., and van den Broeke, M. R.: Application of GRACE to the assessment of model-based estimates of monthly Greenland Ice Sheet mass balance (2003–2012), The Cryosphere, 10, 1965–1989, doi:10.5194/tc-10-1965-2016, 2016.

van Angelen, J. H., van den Broeke, M. R., and van de Berg, W. J.: Momentum budget of the atmospheric boundary layer over the Greenland ice sheet and its surrounding seas, J. Geophys. Res., 116, D10101, doi:10.1029/2010JD015485, 2011.

van Angelen, J. H., Lenaerts, J. T. M., Lhermitte, S., Fettweis, X., Kuipers Munneke, P., van den Broeke, M. R., van Meijgaard, E., and Smeets, C. J. P. P.: Sensitivity of Greenland Ice Sheet surface mass balance to surface albedo parameterization: a study with a regional climate model, The Cryosphere, 6, 1175–1186, doi:10.5194/tc-6-1175-2012, 2012.

van den Broeke, M. R., Enderlin, E. M., Howat, I. M., Kuipers Munneke, P., Noël, B. P. Y., van de Berg, W. J., van Meijgaard, E., and Wouters, B.: On the recent contribution of the Greenland ice sheet to sea level change, The Cryosphere, 10, 1933–1946, doi:10.5194/tc-10-1933-2016, 2016.

Van Tricht, K., Lhermitte, S., Lenaerts, J. T. M., Gorodetskaya, I. V., LEcuyer, T. S., Noël, B., van den Broeke, M. R., Turner, D. D., and van Lipzig, N. P. M.: Clouds enhance Greenland ice sheet meltwater runoff, Nat. Commun., 7, 10266, doi:10.1038/ncomms10266, 2016.

Vernon, C. L., Bamber, J. L., Box, J. E., van den Broeke, M. R., Fettweis, X., Hanna, E., and Huybrechts, P.: Surface mass balance model intercomparison for the Greenland ice sheet, The Cryosphere, 7, 599–614, doi:10.5194/tc-7-599-2013, 2013.

Wyard, C., Scholzen, C., Fettweis, X., Van Campenhout, J., and François, L.: Decrease in climatic conditions favouring floods in the south-east of Belgium over 1959–2010 using the regional climate model MAR, Int. J. Climatol., 37, 2782–2796, doi:10.1002/joc.4879, 2017.